Published in final edited form as:
Neuroscience. 2015 January 29; 0: 166–193. doi:10.1016/j.neuroscience.2014.10.057.

Heterotypic gap junctions at glutamatergic mixed synapses are abundant in goldfish brain

John E. Rash[1,2], **Naomi Kamasawa**[3], **Kimberly G. Vanderpool**[1], **Thomas Yasumura**[1], **John O'Brien**[4], **Srikant Nannapaneni**[5], **Alberto E. Pereda**[5], and **James I. Nagy**[6]

[1]Department of Biomedical Sciences

[2]Program in Molecular, Cellular and Integrative Neurosciences, Colorado State University, Fort Collins, CO

[3]Max Planck Florida Institute for Neuroscience, Jupiter, FL

[4]Department of Ophthalmology and Visual Science, University of Texas Health Science Center, Houston, TX

[5]Dominick Purpura Department of Neurosciences, Albert Einstein College of Medicine, Yeshiva University, Bronx, NY

[6]Department of Physiology, Faculty of Medicine, University of Manitoba, Winnipeg, Manitoba, Canada

Abstract

Gap junctions provide for direct intercellular electrical and metabolic coupling. The abundance of gap junctions at “large myelinated club ending” synapses on Mauthner cells of the teleost brain provided a convenient model to correlate anatomical and physiological properties of electrical synapses. There, presynaptic action potentials were found to evoke short-latency electrical “pre-potentials” immediately preceding their accompanying glutamate-induced depolarizations, making these the first unambiguously identified “mixed” (*i.e.*, chemical plus electrical) synapses in the vertebrate CNS. We recently showed that gap junctions at these synapses exhibit asymmetric electrical resistance (*i.e.*, electrical rectification), which we correlated with total molecular asymmetry of connexin composition in their apposing gap junction hemiplaques, with Cx35 restricted to axon terminal hemiplaques and Cx34.7 restricted to apposing Mauthner cell plasma membranes. We now show that similarly heterotypic neuronal gap junctions are abundant throughout goldfish brain, with labeling exclusively for Cx35 in presynaptic hemiplaques and exclusively for Cx34.7 in postsynaptic hemiplaques. Moreover, the vast majority of these asymmetric gap junctions occur at glutamatergic axon terminals. The widespread distribution of heterotypic gap junctions at glutamatergic mixed synapses throughout goldfish brain and spinal

Address for e-correspondence: john.rash@colostate.edu.

Conflict of Interest: None.

cord implies that pre- *vs.* postsynaptic asymmetry at electrical synapses evolved early in the chordate lineage. We propose that the advantages of the molecular and functional asymmetry of connexins at electrical synapses that are so prominently expressed in the teleost CNS are unlikely to have been abandoned in higher vertebrates. However, to create asymmetric coupling in mammals, where most gap junctions are composed of Cx36 on both sides, would require some other mechanism, such as differential phosphorylation of connexins on opposite sides of the same gap junction or on asymmetric differences in the complement of their scaffolding and regulatory proteins.

Large myelinated club endings (LMCEs) are identifiable auditory synaptic contacts on teleost Mauthner cells (M-cells) (Bartelmez, 1915; Bodian, 1937). LMCE's of adult goldfish co-express specializations for both chemical and electrical transmission, having 60-260 tightly-clustered gap junctions surrounded by and interspersed among variable numbers of “active zones” in presynaptic membranes, apposed by equal numbers of distinctive glutamate-receptor-containing postsynaptic densities (PSDs) (Tuttle et al., 1986; Nakajima et al., 1987). Collectively, LMCE/M-cell gap junctions consist of up to 106,000 intercellular ion channels per synaptic contact (Tuttle et al., 1986), thereby providing the ultrastructural basis for the first example of electrical coupling observed in the vertebrate central nervous system (CNS) (Robertson et al., 1963; Furshpan, 1964). Presynaptic action potentials in LMCE's trigger a mixed synaptic response composed of a large early electrical component, which is followed immediately (<0.5 mSec) by a longer lasting but smaller glutamate-induced depolarization (Lin and Faber, 1988). Thus, the abundance of gap junctions at these contacts insures a rapid dendritic depolarization, with the resulting M-cell action potential evoking the classic “tail-flip” escape response.

Over a decade ago, we reported that an antibody generated against mammalian connexin36 (Cx36), as well as two other antibodies against teleost connexins that share conserved sequences with human/mouse Cx36 and with both perch Cx35 and perch Cx34.7, resulted in strong freeze-fracture replica immunogold labeling (FRIL) of both pre- and postsynaptic hemiplaques of goldfish LMCE/M-cell gap junctions (Pereda et al., 2003). In contrast, a monoclonal antibody generated against Cx35 that does not recognize Cx34.7 produced immunogold labeling that was exclusively presynaptic (*i.e.*, in LMCE axon terminal hemiplaques) and did not label connexins in postsynaptic (M-cell) hemiplaques. Thus, we called attention to likely “differences between presynaptic and postsynaptic connexins” and noted that “additional connexins may be present” in the postsynaptic hemiplaques at these LMCE/M-cell gap junctions (Pereda et al., 2003). However, at that time, we did not identify Cx34.7 as the postsynaptic connexin because the two antibodies then available against Cx34.7, although useful for FRIL (Flores et al., 2012; Rash et al., 2013), did not yield detectable immunofluorescence labeling of goldfish LMCE/M-cell synapses.

Subsequently, we discovered that LMCE/M-cell gap junctions exhibit moderately-strong electrical rectification [*i.e.*, 4:1 asymmetric coupling resistance (Rash et al., 2013)], but with the unexpected property that conductance is normally greater from the postsynaptic M-cell dendrite into nearby LMCE axon terminals (Fig. 1). Consequently, we proposed that retrograde depolarizations may provide for “lateral excitation” of surrounding LMCE

auditory inputs, thereby facilitating the auditory-evoked tail-flip escape response. Electrical rectification is generally associated with asymmetries in the molecular composition of the contributing gap junction hemiplaques (Palacios-Prado et al., 2014). To investigate for possible molecular asymmetries at LMCE/M-cell, we employed multiple additional non-cross-reacting antibodies to Cx34.7 *vs.* Cx35 (O'Brien et al., 2004), in combination with confocal light microscopic immunocytochemistry, FRIL electron microscopy, and matched double-replica FRIL (DR-FRIL), to show that both of these connexin homologs of mammalian Cx36 are present at all LMCE/M-cell mixed synapses (Rash et al., 2013). However, we found that these connexins have an asymmetric localization to apposing hemiplaques, with Cx35 present only in LMCE axon terminal hemiplaques (Fig. 1; green connexons) and Cx34.7 only in the postsynaptic M-cell somatic and dendritic hemiplaques (Fig. 1; blue connexons). We thus proposed that these heterotypic and therefore asymmetric gap junctions provide a plausible molecular substrate for the electrical rectification observed at these synapses (Rash et al., 2013).

In the current study, we examined the distribution of these same connexin proteins by confocal immunofluorescence microscopy, FRIL, and DR-FRIL in selected regions of goldfish brain to gain insight into the density at which neuronal gap junctions occur in the CNS of these vertebrates and to determine if the above findings and concepts pertaining to the LMCE/M-cell system can be applied to other areas of the teleost CNS. We examined other areas in the FRIL replicas of goldfish hindbrain previously investigated, plus additional regions in new replicas from additional goldfish brains. We now report that Cx35/Cx34.7-containing neuronal gap junctions and their corresponding fluorescent puncta occur abundantly (*i.e.*, several hundred to several thousand fluorescent puncta per individual neuron) in diverse areas of the goldfish brain and rostral spinal cord. Moreover, in >700 immunogold-labeled gap junctions found by FRIL, the vast majority were at axon terminals, forming axo-somatic and axo-dendritic glutamatergic mixed synapses, with none found at GABAergic or glycinergic synapses, and none found at dendro-dendritic appositions. All neuronal gap junctions detected were labeled for Cx35 (but not for Cx34.7) in the hemiplaques of the axon-terminal-side of gap junctions and for Cx34.7 (but not for Cx35) in the hemiplaques of the somatic or dendritic side of junctions; and no hemiplaque was labeled for both connexins. Moreover, Cx35 was found opposite Cx34.7 in all matched hemiplaque pairs found by DR-FRIL. Thus, all Cx35/Cx34.7-containing gap junctions found at mixed synapses in the goldfish brain were molecularly asymmetric in pre- *vs.* postsynaptic sides. With gap junction asymmetry proposed as a requirement for electrical rectification (Auerbach and Bennett, 1969; Oh et al., 1999; Palacios-Prado et al., 2014), the connexin asymmetry observed at Cx35/Cx34.7-containing neuronal gap junctions throughout goldfish brain suggests the potential for widespread electrical rectification in the teleost CNS. In addition, the asymmetry could serve other, still unknown, functional properties of electrical synapses.

Experimental Procedures

Antibodies

In a recent report (Rash et al., 2013), we showed that while several anti-Cx36 antibodies detected both Cx34.7 and Cx35 (*e.g.*, Ab39-4200, from ThermoFisher Scientific, Inc.; formerly Life Technologies/Invitrogen; Carlsbad, CA), we have identified three additional anti-Cx34.7 antibodies that selectively detect Cx34.7 but not Cx35 (Cx34.7 CT chicken [JOB 1263-2], Cx34.7 IL rabbit [2930-1 and 2930-2]), and four that selectively detect Cx35 but not Cx34.7 (MAB3045, MAB3043, Ab37-4600, and Ab51-6300) (Table). Of these, all except Cx34.7 CT and Cx34.7 IL are available commercially, either from ThermoFisher Scientific [Ab37-4600, and Ab51-6300] or from Millipore [Biosciences Research Reagents, Temecula, CA; MAB3045, MAB3043]. Limited amounts of Ab298 are available directly from Dr. Nagy and, limited amounts of JOB 1263-2, 2930-1 and 2930-2 are available directly from Dr. O'Brien).

Each of these antibodies has been characterized previously for specificity of connexin detection, including by use of Cx36 knockout mice to show absence of labeling with those antibodies generated against Cx36 (Li et al., 2004; Rash et al., 2013). In this report, we show immunofluorescence images of tissues labeled with Ab39-4200 and FRIL images labeled with monoclonal anti-Cx35 (MAB3043 and MAB3045; Millipore) and polyclonal anti-Cx34.7 IL (2930-1 and 2930-2). [See Yao et al. (2014) for postsynaptic labeling of M-Cell with chicken anti-Cx34.7 CT and rabbit anti-Cx34.7 IL in zebrafish]. In addition, several samples were double-, triple-, or quadruple-labeled for Cx32, Cx43, Cx36, and NMDAR1 (n-methly-D-aspartate receptor subunit 1), including: NMDAR1 + Cx36 (Ab298); and Cx32+Cx36, followed by Cx43+NMDAR1 [sequential labels were: Cx32r + Cx36m (1hr) → 18r+6m+12m (12hr) → rinse → Cx43r + NMDAR1 m (1 hr) → 12r + 18m (24hr)]) (r = rabbit polyclonal antibody; m = mouse monoclonal antibody).

Immunofluorescence labeling for Cx35 and Cx34.7

To assess the relative density of Cx34.7/Cx35-containing gap junctions in various region of adult goldfish brain and spinal cord, 12 adult goldfish 8-9 cm in length were used for immunofluorescence labeling with antibody Ab39-4200, which detects both of these connexins. Fish were deeply anesthetized with 0.08% tricane methanesulfonate (aka MS-222; Argent Chemical Laboratories, Redmond, WA) until cessation of gill movement, then placed on an ice tray. Whole brains, from telencephalon to the rostral spinal cord, were removed and placed for 60 to 90 min into fixative consisting of 0.16 M sodium phosphate buffer, pH 7.2, containing 0.2% picric acid and 1% formaldehyde diluted from a 20% stock solution (Electron Microscopy Sciences, Hatfield, PA, USA). Brains were then transferred to cryoprotectant containing 25 mM sodium phosphate buffer, pH 7.4, 10% sucrose and 0.04% sodium azide and kept at 4°C for 24-48 h. Horizontal sections of the entire length of brain and rostral spinal cord were cut at a thickness of 10-15 μm using a cryostat and collected on gelatinized glass slides. Slide-mounted sections could be routinely stored at -35°C for several months before use. Slide mounted sections were removed from storage, air dried for 10 min, washed for 20 min in 50 mM Tris-HCl, pH 7.4, containing 1.5% sodium chloride (TBS), 0.3% Triton X-100 (TBSTr), and processed for immunofluorescence

staining. Sections were incubated for 24 h at 4 °C with anti-Cx36 Ab39-4200 primary antibody at a concentration of 2 μg/ml diluted in TBSTr containing 10% normal donkey serum, then washed for 1 h in TBSTr and incubated for 1.5 h at room temperature with Cy3-conjugated donkey anti-mouse immunoglobulin G (IgG) as secondary antibody (Jackson ImmunoResearch Laboratories, West Grove, PA, USA) diluted 1:600 in TBSTr containing 10% normal goat serum or 10% normal donkey serum. Some sections processed for immunolabeling were counterstained with Blue Nissl NeuroTrace (stain N21479; Molecular Probes, Eugene, OR, USA). All sections were coverslipped with antifade medium Fluoromount-G (SouthernBiotech, Birmingham, AB, USA), and were either viewed immediately or were stored at −20°C until taken for examination. Immunofluorescence was examined on a Zeiss Imager Z2 microscope and a Zeiss 710 laser scanning confocal microscope, using Zeiss ZEN Black image capture and analysis software (Carl Zeiss Canada, Toronto, Ontario, Canada). Data from wide-field and confocal microscopes were collected either as single scan images or z-stack images, with multiple optical scans capturing a thickness of 4 to 7 μm of tissue at z scanning intervals of 0.4 to 0.6 μm. Final images were assembled using CorelDraw Graphics (Corel Corp., Ottawa, Canada) and Adobe Photoshop CS software (Adobe Systems, San Jose, CA, USA). Two of the figures presented here (*i.e.*, Figs. 2A, 3A) are photomontages consisting of 54 and 32 separate images, respectively, captured using the Zeiss Imager Z2 with a ×20 objective lens, and stitched together using Zen software. These images have been deposited to the Cell Centered Database (http://ccdb.ucsd.edu) and may be viewed at greater resolution using high zoom factor.

Counts of immunofluorescent puncta representing immunolabeling for Cx34.7 and/or Cx35 with Ab39-4200 were conducted for those puncta associated with presumptive reticulospinal neuron (RSN) somata and, where present, their initial dendritic segments. High-resolution confocal images were captured using a ×40 or ×60 oil immersion objective lens, with multiple z-scans encompassing tissue thickness ranging from 0.43 μm to 10 μm. Maximum intensity projections of images were then displayed on a monitor at high magnification to visualize individual neurons. Counts of puncta were conducted manually with the aid of clear acetate overlays applied to the monitor to record individually identified puncta. Images of z-stacks rather than single scans were used for counts in order to avoid repeated counts of portions of the same puncta that appeared in each of two adjacent scans.

Separate labeling for Cx34.7 and Cx35 in reticulospinal and in vestibulospinal neurons

Following anesthesia, goldfish brains were removed and fixed in 1% formaldehyde containing 0.2% picric acid. The brains were transferred after 1 h into 30% sucrose solution and stored at 4°C for 18-20 h. Sections of 50-μm thickness were obtained using a cryostat (maintained at −24°C). The sections were collected on slides, allowed to dry for 2-3 h and then rinsed in sodium phosphate buffered 0.9% saline (PBS). After blocking for 1 h in PBS containing 10% normal goat serum and 0.5% Triton X-100, the sections were incubated overnight at 4°C with rabbit polyclonal anti-Cx34.7 IL and mouse monoclonal anti-Cx35 (Chemicon MAB3043) antibodies. Sections were then washed in 0.4% Triton in 1× PBS and incubated with Alexa Fluor 488-conjugated goat anti-rabbit and/or Alexa Fluor 594-conjugated goat anti-mouse secondary antibodies for 1 h at room temperature. Finally, the

sections were washed in 0.1-0.4% Triton in PBS, and coverslipped using n-propylgallate-based mounting media. Sections were then imaged using an Olympus BX61WI confocal microscope. Confocal immunofluorescence XY images were scanned in Z-axis intervals of 0.2-0.8 μm. Selected imaged images were processed using Adobe Photoshop (Adobe Systems, San Jose, Ca) and Canvas X (ACD Systems) for presentation purposes.

Preparation of tissue slices for single-replica FRIL and double-replica SDS-FRL

As previously detailed (Pereda et al., 2003), goldfish Mauthner cells were injected with Lucifer Yellow, the fish were fixed by perfusion with 1% formaldehyde in fish Ringer's solution (pH 7.4), and the brains were sliced with a refrigerated Vibratome® to uniform 150-μm thickness, which facilitates predictable sample-cleaning (*i.e.*, detergent-washing) times, as required for FRIL (Rash and Yasumura, 1999). Thick sections were photomapped by confocal microscopy, then infiltrated with 30% glycerol as a "cryoprotectant", which eliminates ultrastructurally-detectable ice-crystals that otherwise would form during specimen freezing (Haggis, 1961). Slices of hindbrain from rhombomeres R2-R5 (Metcalfe et al., 1986; Hanneman et al., 1988) were closely trimmed to contain primarily RSN and vestibulospinal neurons (Eaton et al., 1977; Lee et al., 1993). Each slice included a portion of a single fluorescently-injected M-cell (left or right side). Slices were placed on aluminum "Slammer" supports (Chandler and Heuser, 1979), frozen by contact with a liquid nitrogen-cooled copper block, and stored in liquid nitrogen until fractured.

Conventional FRIL

Coronal slices of goldfish midbrain and hindbrain were infiltrated with 30% glycerol and frozen as above. Frozen slices were knife-cleaved in either a JEOL/RMC JFD 9010C or JFD II freeze-fracture device equipped with a −170°C liquid-nitrogen-cooled specimen cryoshroud and a liquid-helium-cooled cryopump (Rash and Yasumura, 1999). Freeze-fractured samples were either coated with 1-5 nm of carbon before replication [to increase labeling efficiency (Fujimoto, 1995; Schlörmann et al., 2007) but also decreases image resolution], or were replicated with 1-2 nm of platinum immediately after fracture (Rash and Yasumura, 1999). All replicated samples were stabilized by coating with 10-20 nm of carbon; the samples were removed and placed into a liquid nitrogen-cooled-cooled chamber that maintained the atmosphere at *ca.* −180°C; and except for matched double-replica samples (see below), a 200-mesh gold "index" grid suspended in a droplet of 3% Lexan dissolved in dichloroethane was placed on each replicated but still frozen surface (Steere and Erbe, 1983; Rash and Yasumura, 1999). The solvent was allowed to harden ("freeze") by cooling to −180°C; the replicated tissue-grid-Lexan "sandwich" was placed in a −25°C freezer compartment; and the solvent was allowed to melt (−35°C) and to evaporate overnight at −25°C. The tissue within the replicated samples was thawed to room temperature, photomapped by confocal microscopy, and the bulk of the tissue was then washed from the replica by suspending the "sandwich" in 2.5% sodium dodecyl sulfate (SDS) detergent and rocking gently for 29 h at 60°C (Pereda et al., 2003). Samples were rinsed in distilled water, then rinsed for a minimum of 30 min in "labeling blocking buffer" (LBB), which consists of 1.5% fish gelatin digest plus 10% heat-inactivated goat serum (Dinchuk et al., 1987). After blocking of non-specific binding sites by LBB, replicated samples were double- or triple-labeled for 4-6 h using rabbit anti-Cx34.7 antibody (2930-I),

with or without chicken anti-Cx34.7 CT antibody (JOB #1263), plus mouse monoclonal MAB3043 and MAB3045 against Cx35 (see Table of antibodies used by LM *vs.* FRIL). Labeled replicas were then counter-labeled for 16 h with 5-nm, 10-nm, 20-nm, or 30-nm gold coupled to goat anti-rabbit or goat anti-mouse antibodies (BBI Solutions) and 6-nm, 12-nm, and/or 18-nm gold coupled to goat anti-rabbit or goat anti-mouse, and 12-nm gold coupled to goat anti-chicken antibodies (Jackson ImmunoResearch), or the samples were double-, triple-, or quadruple labeled as described below. The use of multiple sizes of gold for each primary antibody provides multiple independent internal confirmations of labeling specificity and labeling efficiency of primary antibodies and of labeling efficiency for each secondary antibody; and the highly visible larger gold beads, when confirmed to label effectively, allowed searching at lower magnification (5,000×) for labeled gap junctions (Kamasawa et al., 2006).

Sequential labeling for four proteins

One sample was triple-labeled, first with mouse anti-Cx36/anti-Cx35 (Ab37-4600) followed by goat anti-mouse 6-nm and 12-gold beads, then after rinsing, mouse antibodies to NMDAR1 and rabbit anti-Cx43 were applied and counter-labeled by goat anti-mouse 18-nm gold beads and goat anti-rabbit 12-nm gold beads. (Note that the two mouse antibodies were used sequentially, with copious rinsing between labeling steps.) Because of incomplete occupation of the initial mouse monoclonal anti-Cx35 antibody by 6-nm and 12-nm gold-conjugated goat anti-mouse secondary antibodies, and after washing and sequential application of the second mouse anti-NMDAR1 antibody, followed by a second goat anti-mouse antibody conjugated to 18 nm gold, only 18-nm gold beads label the glutamate receptor clusters, but additional immunogold labeling occurred on unoccupied sites on mouse anti-Cx35, resulting in all three sizes of gold (6-nm, 12-nm, and 18-nm gold) on Cx35-containing gap junctions. In addition to entirely different morphologies of gap junctions *vs.* glutamate receptor PSDs, this labeling of NMDAR1 by 18-nm gold beads, only, *vs.* labeling of Cx35 by 6-nm and 12-nm gold and then by 18-nm gold beads (three sizes) provides further insight into the specificity and complex nature of sequential immunogold labeling methods, including the fact that even though they were labeled for 12 hours with secondary antibodies coupled to smaller gold beads (6-nm and 12-nm) with presumably higher labeling efficiency, many Cx35 antibody-binding sites remained unoccupied and available for subsequent strong labeling by 18-nm gold beads (see RESULTS). [Note: Astrocyte gap junctions were weakly labeled by 12-nm gold beads for Cx43 (not shown), and were thus readily distinguishable from neuronal gap junctions, which were strongly labeled by all three sizes of gold (see RESULTS).]

Sources of search bias in FRIL samples that are well-labeled for Cx35/Cx34.7

To minimize investigator bias in quantifying relative abundance of particular types and locations of gap junctions labeled for Cx35 (see below for caveat regarding Cx34.7), we examined all replicated areas of gray and white matter at a transmission electron microscope magnification too low to recognize gap junctions, instead searching solely for the larger gold beads used in a particular labeling strategy. For example, we view at 5,000× (with ×10 binocular viewer) for 18-nm, 20-nm, and 30-nm gold beads and at 10,000× (×10) for 10-nm and 12-nm gold beads. Because 5-nm gold beads are visible only at magnifications greater

than 30,000x (x10), in searches of uncharacterized tissues, 5-nm gold beads were used only in combination with a larger size of beads – for example 5-nm and 20-nm gold beads to label one connexin, paired with 10- and 30-nm gold beads to label a second connexin. Only when 5-nm gold beads labeling a particular connexin are confirmed to label a particular type of apposition (*e.g.*, LMCE/M-cell and RSN synapses) do we search for appropriate cytological markers, then increase magnification to identify gap junctions. For example, at 5,000×, we were able to recognize cross-fractures of the large-diameter cell bodies of M-cells [see Fig. 2A in Rash et al., (2013)], then search their peripheries at higher magnification for LMCE synapses labeled by 5-nm or 10-nm gold. Moreover, in the areas of replica that we were able to search (see time constraints, below), we examined all areas of neuropil and cellular gray matter for potential immunogold labeling. This search strategy insured that all neuronal and non-neuronal areas in selected grid openings are searched, without bias as to cell type or labeled protein. By first determining that the appropriate primary and secondary labels are functioning properly (Rash and Yasumura, 1999), this search strategy allows determination of the relative abundance of Cx35-containing gap junctions at different neuronal subcellular locations. In contrast, and for unknown technical reasons, antibody labeling for Cx34.7 was highly variable from sample to sample and antibody to antibody, from strong to non-existent. In samples moderately or well labeled for Cx34.7 (*e.g.*, samples designated “811” and “DR-FRL top and bottom”), counts and specific locations for Cx34.7 were considered reliable (*i.e.*, always and only in somatic and dendritic hemiplaques and never in axon terminal hemiplaques). However, in several other samples, labeling for Cx35 was strong and reliable but labeling for Cx34.7 was weak or nonexistent in nearby postsynaptic hemiplaques, which remained unlabeled for either connexin (see RESULTS). In those samples where antibodies to Cx34.7 were ineffective, postsynaptic views were infrequently recognized by this method, substantially biasing the results in those samples by potentially precluding recognition of dendro-dendritic gap junctions composed exclusively of Cx34.7 on both sides of the junctions, if such gap junctions exist in goldfish midbrain and hindbrain (see RESULTS and DISCUSSION).

Limitations on examining all searchable areas of FRIL replicas

A typical FRIL replica is 1.5 × 1.5 mm (or 2.25×10^6 μm^2). At 10,000× magnification, we are able to scan *ca.* 1 μm^2 per second (one optical field per second). To examine an entire replica would require 2.25×10^6 seconds or 84 eight-hour days – an impossible task if we wish to examine large numbers of replicas. Consequently, when available, we use confocal photomaps to limit the areas searched to selected brain sub-regions. Nevertheless, several well-labeled smaller replicas were examined in their entireties.

Matched double-replica SDS-FRL and double-replica FRIL

For double-replica SDS-FRL (DR-SDS-FRL) (Li et al., 2008), tissue slices were dissected to *ca.* 1.5 mm diameter and placed within a “donut” of 150-μm-thick double-stick tape previously bonded to a Balzers 4.5 mm-diameter gold specimen support. A second gold specimen support, with or without a thin film of 10% polyvinyl alcohol in 30% glycerol (Cohen and Pumplin, 1979) was placed on top, and the double-replica “sandwich” was frozen by plunging into liquid propane held at its freezing point (*ca.* −188°C) in liquid nitrogen. [Polyvinyl alcohol is used as a fracture-resist on both sides to prevent the fracture

from occurring outside the tissue slice.] To further decrease the probability that the fracture plane would follow the lipid-coated surface of the tissue slices, some samples were rinsed briefly in SDS detergent, then frozen as above. [A film of displaced lipids often forms during or immediately following Vibratoming, even when the slices of these cold-blooded animals were maintained at 4 °C during Vibratoming (Rash and Yasumura, unpublished observation). This lipid film, when present, provides a protein-free layer on the surface of the slice, which preferentially cleaves in DR samples, preventing fracturing of the tissue.] One DR sample was placed in a JEOL double-replica stage and fractured at −105°C and etched for 5 min in the final factory prototype of the JEOL JFD-2 freeze-fracture device, then replicated with 2-4 nm of carbon and 1.5-2 nm of platinum, followed by 20-nm of evaporated carbon. The samples were thawed and floated free for washing and labeling. DR-SDS-FRL samples were washed for 29 h at 80°C in 2.5% SDS detergent. One set of matched double-replica pairs (designated “DRD top” and “DRD bottom”) was labeled simultaneously for 4 h at room temperature with rabbit polyclonal antibody against Cx34.7 (JOB #2930/2) and mouse monoclonal antibody directed against Cx35 (O'Brien et al., 1996; O'Brien et al., 2004) (Chemicon/Millipore MAB3045), then counter-labeled overnight at room temperature with goat anti-rabbit IgG conjugated to 5-nm gold beads and goat anti-mouse IgG conjugated with 10-nm gold. After labeling, samples were rinsed and picked up on Formvar-coated 75-mesh gold index grids, and air dried.

After labeling, all samples were inverted and the labeled tissue-side of the replica (“inverse side”) was coated with a thin layer (*ca.* 20 nm) of vapor-deposited carbon prior to removing the Lexan support film. (DRD samples were mounted on Formvar films and not coated with Lexan, obviating removal of Lexan films.) This additional carbon coat was applied to anneal cracks created in the replica by thermal expansion during warming from liquid nitrogen to room temperature (a change of *ca.* +220°C) and to immobilize and stabilize gold labels on the inverse side. For all samples except “DRD top” and “DRD bottom” (which were not coated with Lexan), the Lexan support film was removed by gentle rinsing for 24 h in dichloroethane, and the labeled replicas were air dried.

Electron microscopy

Replicas were examined in JEOL JEM 2000 EX-II, JEOL JEM 1400, and JEM 1200 EX transmission electron microscopes (TEMs) operated at 100 kV. Images were obtained at 55×-1000× magnification for correlation with light microscopic photomaps; at 5,000 or 10,000× to map gold “flagged” gap junctions and to identify fiduciary marks in mirror image complements; and as stereo pairs at 30,000× or 50,000× to analyze “sidedness” of gold labeling and to match mirror-image complements of individual gap junction hemiplaques. Replicas were rotated so that the original shadowing azimuth was approximately parallel to the direction of specimen tilt, allowing shadow contrast and definition to be optimized (Steere and Rash, 1979). All neuronal gap junctions encountered were photographed as stereo pairs having an 8° included angle. TEM negatives from the JEOL 2000 and 1200 TEMs were digitized at 1200 dpi (*ca.* 16 megapixels) using ArtixScan 2500 and 2500f digital scanners, whereas digital images were directly captured using an 11 MB Orius camera on the JEOL 1400 TEM. Digitized images were prepared using Photoshop CS5, with “Levels” used to adjust contrast and brightness and to expand the

contrast range to utilize the entire grayscale. Large-area “dodging” was used to reduce extremes of local brightness or to bring out areas of reduced brightness, as under displaced carbon flakes. Selected images are presented as stereo pairs to demonstrate proper “sidedness” of labels (Rash and Yasumura, 1999). To allow image cropping for rectangular margins, as is required for optimum stereopsis, and to compensate for minor image distortion in the z axis created during initial electron microscopic image recording at two different tilt angles, the stereo windows were made to appear square and level using the “Distort” function of Photoshop.

Results

Immunofluorescence imaging of Cx34.7/Cx35

Brainstem—Immunofluorescence labeling for neuronal connexins in horizontal sections of goldfish brain was conducted with Ab39-4200, which detects both Cx34.7 and Cx35. The results presented here are not meant to represent detailed mapping or cellular characterization of these connexins. Our previous studies focused specifically on the association of Cx35 and Cx34.7 with M-cell and their club endings (Rash et al., 2004, 2013), so we begin here by an examination of labeling for these connexins in the brainstem. In addition to the spinal projections of M-cell, several other groups of RSNs located rostral and caudal to these cells have been described and were considered segmentally homologous (Metcalfe et al., 1986; Hanneman et al., 1988). In particular, groups of RSNs in the reticular formation of the goldfish hindbrain were described to be organized in rhombomeres having recognizable segmentation patterns ranging from reticulospinal segment 1 (RS1) to RS7 or putative RS8, with RS4 representing the group containing the M-cell (Lee et al., 1993). Shown in Figure 2A (abundant red fluorescence) is labeling for Cx34.7/Cx35 with Ab39-4200 at a rostral level of the hindbrain revealing the prominent lateral dendrite of M-cell, with its typical pattern of labeling for these connexins distributed in patches along the dendrite (Fig. 2B), consistent with labeling of these connexins with other anti-Cx34.7 and Cx35 antibodies (Rash et al., 2013). The numerous individual gap junctions (*i.e.*, immunofluorescent puncta) associated with each patch are not separately resolvable in the low magnification images shown. At levels rostral and caudal to the M-cell lateral dendrite (Fig. 2A), labeling of these connexins was equally dense to that in the area of the M-cell, as shown at higher magnification in Figures 2C and 2D, respectively. This labeling was in part associated with the somata and dendrites of medium and large neurons that presumably correspond to those in rostral and caudal rhombomere segments having reticulospinal projections, according to the nomenclature of Lee et al. (1993). Although the dense labeling shown in the low magnification photomontage in Figure 2A could be mistaken to arise from a low signal-to-noise ratio, background signal was relatively low and all labeling had an exclusively punctate appearance that is typical of connexins associated with gap junctions, as shown at higher magnifications (Fig. 2E-F). Further, punctate labeling was localized to the surface of neurons, with no intracellular labeling detectable by confocal through-focus examination of neuronal somata and their large initial dendrites.

Hindbrain—Immunolabeling for Cx34.7/Cx35 in a horizontal section of goldfish hindbrain just caudal to the M-cell and extending caudally to the interface with the spinal cord is

shown in Figure 3A. As described by Lee et al. (1993), rostral areas in this section marked with a single asterisk (Fig. 3A) correspond to RS5-7, a mid-region marked with double asterisks (Fig. 3A) containing a column of neurons appears to correspond to RS8, and the caudal area represents a transition to the spinal cord. In all of these regions, medially located neuronal somata of different shapes and sizes, as well as their laterally-directed dendrites, were heavily immunolabeled for Cx34.7/Cx35. In each region, labeling was exclusively punctate and localized to neuronal surfaces (Fig. 3B-D).

Quantitative confocal microscopic analysis—To obtain estimates of the density of Cx34.7/Cx35-puncta associated with presumptive RSNs, images were taken for counts of these puncta covering the surface of large neuronal somata and their initial dendrites (Fig. 3E-G). A total of 47 individual neurons displaying a cumulative total of 10,247 puncta in images with z-18 scan dimensions ranging from 0.43 to 10 μm were examined. The number of puncta covering individual neurons ranged from 50 to 566, with this variability being due in large part to differences in z-scan thicknesses in different images. When normalized to puncta/μm in the z dimension, the number of puncta per 1 μm section thickness of neuronal soma and initial dendrite ranged from 13 to 188, with a mean ± s.e.m. of 75 ± 11 per μm thickness. This suggests that RSN neuronal somata having typical diameters of 25 to 50 μm each have as many as 1875 to 3750 puncta associated with their cell bodies and initial dendrites, not including those puncta on their more distant extensive dendritic arbors, which were not counted due to technical limitations of serial-section reconstruction and alignment. It is unlikely that these numbers (1875-3750 puncta) reflect the number of axon terminals having single gap junctions because FRIL (see below) reveals up to 30 gap junctions per axon terminal on RSN, suggesting that there may be far few terminals having single gap junctions, with many having 10-30 gap junctions per terminal.

Variable labeling in forebrain and midbrain—Examples of immunolabeling for Cx34.7/Cx35 in selected forebrain and midbrain regions are shown in Figure 4, including the dorsal telencephalon (Fig. 4A), optic tectum (Fig. 4B), vagal lobe (Fig. 4C), cerebellum (Fig. 4D), and torus semicircularis (Fig. 4E-F). Unlike immunolabeling in the hindbrain, labeling around neuronal somata was less evident in most regions, and typical punctate labeling appeared to be more heavily distributed in the neuropil. An exception to this was a very high density of immunofluorescent puncta on a subpopulation of neuronal somata in the torus semicircularis (Fig. 4E), whereas labeling elsewhere in this structure was otherwise quite sparse. This, and indeed all labeling in the forebrain, midbrain, and hindbrain regions examined, was exclusively punctate (Fig. 4F; from torus semicircularis; also Fig. 2F). The distribution patterns of puncta encountered were remarkably diverse, ranging from: association with tortuous or radially directed dendrites in the dorsal telencephalon (Fig. 4A); dense collections of coarse as well as sparsely distributed fine puncta in the tectum (Fig. 4B); laminar arrangements of widely distributed puncta in the vagal lobe (Fig. 4C); and isolated patches of puncta in the granule layer of the cerebellum (Fig. 4D).

Immunofluorescence co-localization of Cx34.7 with Cx35

We previously reported confocal immunofluorescence microscopic images showing near precise co-localization of Cx34.7 with Cx35 at LMCE/M-cell synapses (Rash et al., 2013).

To determine whether Cx35 co-localizes with Cx34.7 in individual synapses in other brainstem regions of goldfish, we performed double immunofluorescence labeling using an anti-Cx35 antibody (Chemicon MAB3043) and an anti-Cx34.7 IL antibody (JOB) (see Table). Both Cx35 and Cx34.7 antibodies showed intense punctate staining and, although not completely overlapping, the two proteins exhibit a high degree of co-localization in vestibulospinal and in RSNs (Fig. 5) near the Mauthner cell lateral dendrite. In general, however, immunofluorescence labeling with currently available anti-Cx34.7 antibodies in some samples was either not detected above background autofluorescence or was only weakly detected in some puncta, indicating that fluorescence labeling efficiency of Cx34.7 in cryosections of formaldehyde-fixed tissues may be lower than that of Cx35, possibly due to epitope masking or other labeling fault. As we previously showed in LMCE/M-cell synapses, the limit of resolution of light microscopy (*ca.* 0.2 μm in the blue wavelength and 0.4 μm in the red wavelength) precluded determination of whether Cx35 and Cx34.7 were present in both apposed hemiplaques or were separately segregated to pre- *vs.* postsynaptic hemiplaques. Consequently, we examined for connexin asymmetry in those few FRIL replicas in which labeling for both Cx35 and Cx34.7 was definitive.

Cx34.7 and Cx35 in conventional FRIL replicas

Overview—By freeze fracture, LMCE/M-cell synapses exhibit up to 160 dense clusters of hexagonally-packed 9-nm intramembrane particles (IMPs, or simply “particles”) in the protoplasmic leaflet or “P-face” (Tuttle et al., 1986; Nakajima et al., 1987), representing the freeze-fracture correlate of gap junctions (Fig. 6). Likewise, in the extraplasmic leaflet or “E-face”, equal numbers of distinctive hexagonally-packed clusters of 8-nm intramembrane “pits” are revealed, representing the physical impressions where gap junction connexon particles had been removed during membrane splitting. Here, we use the internationally-recognized freeze-fracture nomenclature of Branton et al. (1975) for designating membrane fracture faces. In contrast to gap junctions in invertebrate species, wherein the fracture plane does not separate apposed innexin particles but instead yields IMPs that contain protein from both apposed cells (Peracchia, 1973a; Peracchia, 1973b), the fracture plane in all vertebrate species separates connexon pairs at their points of contact in the extracellular space (Fig. 6A), resulting in 100% fractionation of connexons in each gap junction (Fig. 6B vs. Fig. 6C), allowing the connexins of each cell to be labeled separately and therefore identified unambiguously, without the possibility of contamination by connexins in one hemiplaque by those in the apposed hemiplaque (Fujimoto, 1995; Fujimoto, 1997; Rash et al., 2001). The blue line labeled “Fig. 9” in Figure 6A and the numbered blue boxes in Figures 6B-C show locations of fractures depicted in Figs. 7, 8,9).

Simultaneous double-labeling using five sizes of gold beads—Previously, we showed high-efficiency triple-immunogold labeling for Cx35, localized solely to presynaptic connexons in both LMCE/M-cell synapses and in nearby RSNs in goldfish hindbrain [Fig. 7A, which is a higher magnification view of Figure 8A,B in Pereda et al (2003)]. In this image, three sizes of gold beads (6-nm, 18-nm, and 20-nm gold beads) were used to label Cx35. Notably, the Cx35-labeled gap junctions did not contain any of the other two sizes of gold beads that were used to simultaneously label Cx34.7 (*i.e.*, 10-nm and 12-nm gold beads; none present). However, in the same replica, 81 additional gap junction postsynaptic

hemiplaques, mostly in the M-cell (Fig. 7B,C) but also in nearby RSNs (Lee et al., 1993), were weakly but positively labeled for Cx34.7 using two other sizes of gold beads (Fig. 7C; 10-nm gold against JOB 2930/l and 12-nm gold beads against JOB 1263-2; see EXPERIMENTAL PROCEDURES). Of these, 49 of 81 hemiplaques (60%) were labeled, and 32 (40%, most containing fewer than 50 connexons) were unlabeled (Fig. 7B). Moreover, none of these postsynaptic hemiplaques (0%) were immunogold labeled for Cx35 (6-nm, 18-nm, and 20-nm gold beads; none present). This clear separation of labels to pre- *vs.* postsynaptic hemiplaques provides strong evidence for differential distribution of the two connexin homologs. Statistical analysis of such disparate ratios would provide little additional information regarding labeling of pre- vs. postsynaptic hemiplaques. Consequently, we developed matched double replica technologies to examine both sides of individual gap junctions (see below).

Weak labeling for Cx34.7 required development of new antibodies—In our previous studies using the same two primary antibodies (Pereda et al., 2003), immunofluorescence imaging was unable to detect Cx34.7 above “background” at LMCE/M-cell synapses, casting some doubt as to the basis for the weak but positive FRIL labeling of Cx34.7 in postsynaptic hemiplaques (Fig. 7B-C). To address this issue, we developed several new antibodies for both Cx35 (MAB3043 and MAB3045; plus two antibodies [Ab37-4600 and Ab51-6300 made against Cx36 that also recognize Cx35 but not Cx34.7]), and additional antibodies against Cx34.7 (Cx34.7 CT and Cx34.7, IL/JOB2930/1) that lack cross-reactivity with Cx35, with both of the Cx34.7 antibodies providing variable (absent to weak to moderate) labeling by both immunofluorescence and FRIL methods (see Table). In combination with newly-developed matched double-replica technology for use in SDS-FRL (Li et al., 2008) and DR-FRIL (Rash et al., 2013), at last one of these additional antibodies provided unequivocal evidence for pre- *vs.* postsynaptic labeling specificity and allowed definitive reinvestigation of both Cx34.7 and Cx35 in a wide variety of mixed synapses in selected areas of goldfish brain.

Matched DR-SDS-FRL and matched DR-FRIL of Cx35 and Cx34.7

In a sample that was prepared as matched double-replicas, both fracture complements were simultaneously double-labeled for Cx35 (10-nm gold beads) and Cx34.7 (5-nm gold beads). In addition to the previously-described LMCE/M-cell synapses (Rash et al., 2013), 10 additional RSN were found >200-500 μm away from the M-cell, in rhombomeres R2-R6, three of which are illustrated in Figure 8B (blue overlays). For correlation with light microscopic images (Fig. 8A, enlarged from Fig. 2F), three other RSN are shown at the same magnification as Figure 8C. On the 10 freeze-fractured RSN, we found from four to 24 small to large CEs, each displaying from one to 32 gap junctions. Almost all of these were within positively identified glutamatergic mixed synapses, as described next.

Criteria for identifying mixed synapses

Excitatory synapses—In FRIL images, excitatory mixed synapses (primarily glutamatergic synapses) on RSN and other unidentified neurons were positively identified by the presence of one or more (up to 32) gap junctions (the electrical component) within synaptic contacts that displayed at least two of the following additional ultrastructural and

immunocytochemical criteria for identifying the chemical synaptic component: *1)* large-diameter (>1×3 μm) axon terminals [Fig. 8C-G] corresponding to the LMCE that arise from glutamatergic axons of the eight cranial nerve (Diamond and Huxley, 1968), *2)* axon terminals containing >10 uniform-diameter "large" (50-nm) round synaptic vesicles (SV) in the cross-fractured axoplasm (Figs. 9C-D) (Nakajima et al., 1987), identifying them as excitatory chemical synapses and distinguishing them from inhibitory (GABAergic and glycinergic) axon terminals, which contain small (20- to 40-nm) flattened or "pleomorphic" SVs (Nakajima et al., 1987; Peters et al., 1991; Legendre, 2001; Peters, 2014), as further described below; *3)* clear impression of the axon terminal into the somatic or dendritic plasma membrane (Figs. 8-10; 11C), with the gap junction within the delineated synaptic contact; *4)* fracture from axon terminal into the postsynaptic neuron soma or proximal dendrite cytoplasm (Figs. 9C,D; 11B, left side), revealing stacks of widely-spaced Nissl substance (distinctive rough endoplasmic reticulum characteristic of neurons) or Golgi membranes, which are found in neuronal somata and dendrites but not in axons; *5*) distinctive clusters of 10-nm E-face particles in the postsynaptic membrane within 0.03 to 0.15 μm of the gap junction and confirmed to be within the same synaptic contact (Figs. 10B-C; 11A,B; yellow overlays), with these distinctive particle clusters previously shown to correspond to glutamate receptors in both fish and mammals (Tuttle et al., 1986; Nakajima et al., 1987; Rash et al., 2005; Masugi-Tokita and Shigemoto, 2007; Hamzei-Sichani et al., 2012)]; *6*) in appropriately-labeled replicas, these E-face particle clusters were positively identified by immunogold labeling (Fig. 11A, 18-nm gold without 6-nm or 12-nm gold) as containing at least a few NMDAR1 glutamate receptors (Pereda et al., 2003); *7)* equally distinctive clusters of pits in postsynaptic P-faces, corresponding to the locations where glutamate receptors particles had been removed during fracturing (Figs. 7B,C and 11C), and *8)* E- or P-face views of one or more active zones in the presynaptic plasma membrane [(Fig. 12B, upper right; see also Nakajima at al. (1987) and Tuttle et al (Tuttle et al., 1986)].

Inhibitory synapses—In contrast to excitatory synapses, GABAergic terminals (Kasugai et al., 2010) and glycinergic terminals (Nakajima et al., 1987), the two primary types of inhibitory synapses, were characterized by *a)* their content of small flattened "pleomorphic" SVs, *b)* distinctive P-face particle clusters in the postsynaptic membrane (Fig. 12), and *c)* their postsynaptic E-faces had clusters of intramembrane pits intermixed with a few 5-nm to 8-nm particles (*i.e.*, particles distinctly smaller, fewer, and less tightly-packed than glutamate receptor particles) (Tuttle et al., 1986; Nakajima et al., 1987). None of many hundreds of inhibitory synapses found in FRIL or DR-FRIL samples was ever found to contain a gap junction, either labeled or unlabeled, as detailed below.

Dendro-dendritic appositions

Dendro-dendritic appositions were identified and distinguished from axo-dendritic synapses based on: *1)* the presence of Nissl substance in either or both cross-fractured dendritic cytoplasms; *2)* the presence of two or more smooth endoplasmic reticulum cisternae (Kosaka, 1983; Kosaka and Hama, 1985; Fukuda and Kosaka, 2000a; Kosaka and Kosaka, 2004; Kosaka and Kosaka, 2005; Fukuda et al., 2006) [but see Sotelo and Korn (1978), who found flattened ER cisternae in most axo-somatic mixed synapses]; *3)* the absence of discernible "active zones" (Pfenninger et al., 1972) [but see Landis and Reese (1974) and

Landis et al. (1974)]; and *4)* absence of clusters of SVs in both processes. To date, no dendro-dendritic appositions having gap junctions have been detected by our FRIL search strategy in either the samples that were well labeled for Cx34.7 (#811 and DRD-top and bottom) or in replicas of other brain regions having strong labeling only for Cx35. However, we emphasize that because available antibodies against mammalian Cx45 and Cx57 have not been shown to share cross reactivities with their teleost homologs, we have not yet attempted FRIL analysis of those connexins in goldfish. Thus, we have no data regarding the existence or localization of Cx45 or Cx57 at inhibitory mixed synapses or at dendro-dendritic synapses in goldfish CNS.

Glutamatergic mixed synapses are abundant on reticulospinal neurons

Four to 24 axon terminals were included in the fracture plane through each of several RSNs (Figs. 8C, 9A), with up to a dozen of these axon terminals corresponding to large and small club endings, while others, based on characteristic ultrastructural features, corresponded to GABAergic and possibly glycinergic inhibitory synapses [see Bodian (1937), Diamond and Huxley (1968), and Legendre (2001) for descriptions of the diverse sizes, functional classes, and partial spatial segregation of the diverse types of synapses found on M-cells]. Complementary double-replicas of one of those large excitatory mixed synapses on RSN is shown at progressively higher magnification (Fig. 8B-G). To standardize descriptions regarding which connexins are labeled beneath E- *vs.* P-faces of pre- *vs.* postsynaptic membranes (four possible views), we describe each labeled gap junction as a view toward the cytoplasm of either the presynaptic or the postsynaptic cell (see Fig. 6B-C). After SDS washing, many of these connexin transmembrane proteins remain for potential labeling of their cytoplasmic epitopes. Connexins are immunogold labeled on these epitopes in the lower cell, whether beneath its P-face particles or beneath E-face pits of the upper cell whose connexons were fractured away. The P-face particles represent platinum-replicated connexons that extend into the cytoplasm of the lower cell, and are labeled on cytoplasmic epitopes and cannot be labeled on the platinum-or carbon-coated extracellular epitopes, even if antibodies existed against those epitopes [for rationale, see Rash et al. (1983)]. In contrast, no connexin protein remains within the gap junction E-face pits; instead, immunogold beads beneath E-face pits are actually bound to connexons of the unfractured membrane of the underlying cell (Fig. 6A-C) (Fujimoto, 1995; Rash and Yasumura, 1999).

Asymmetric labeling of gap junctions at glutamatergic mixed synapses—In a FRIL double-replica, one RSN (Fig. 8C; blue overlay) revealed at least 24 freeze-fractured axon terminals (green overlays). Labeling was for Cx35 but without labeling for Cx34.7 in >30 pre-synaptic hemiplaque P-faces (Figs. 8E,G; 10-nm gold *beads* labeling mouse MAB3045) and for Cx34.7 but without labeling for Cx35 in the matching axon terminal E-face hemiplaques (Figs. 8D,F; 5-nm gold beads; shown diagrammatically as Fig. 6). Overall, in >700 matched and unmatched gap junction hemiplaques from all neurons examined, immunogold beads for Cx34.7 were 100% postsynaptic, including: *a)* beneath the E-face of a large axon terminal but labeling within the postsynaptic RSN (Figs. 8D,F; and shown diagrammatically as Fig. 6C, left side); *b)* beneath the P-face of the neuron soma (Fig. 7B; shown diagrammatically as Fig. 6C, right side); or *c)* beneath areas containing both E-face pits of the axon terminal and P-face particles of the neuron soma (Fig. 7B; shown

diagrammatically as Fig. 6C, combined panels). In one CE/RSN synapse, the E-face of the large CE is viewed toward the RSN (Fig. 8F), with labeling for Cx34.7 in the RSN, whereas the complementary axon terminal P-face (Fig. 8G) is viewed toward the CE, with labeling solely for Cx35 beneath replicated presynaptic connexons. Of the 11 matching gap junction hemiplaques illustrated in Figure 8D-G (numbered 1-11; blue overlays*;* from total of 24 matched gap junctions in that one CE synapse), all are labeled for Cx34.7 (5-nm gold), with no labeling for Cx35; whereas in the P-face of the same CE (*i.e.*, viewed toward the CE), the 11 matching gap junction hemiplaques are labeled for Cx35 (10-nm gold; Fig. 8F; green overlays), with no labeling for Cx34.7. [Lighter ovals (Fig. 8C,D,F) result from holes in the supporting Formvar film that was made during a rare Colorado day having high humidity.]

Asymmetry of connexin coupling confirmed at cross-fractured neuronal gap junctions—In a fracture through neuropil ∼500 μm away from the photomapped M-cell described in Rash et al. (2013) (red line designated “Fig. 9” in Fig. 6B; shown at progressively higher magnifications in Fig. 9), a cross-fractured mixed synapse similar in configuration to a thin-section TEM image was found between an unidentified axon terminal and the soma of an RSN (Fig. 9A), with its identification as the soma of a neuron based on the presence of a cell nucleus (Fig. 9A, pink overlay), 40×60 μm-diameter cell body (blue overlay), and presence of extensive Nissl substance and Golgi membranes (faintly resolvable in Fig. 9B). Stereoscopic imaging (Figs. 9C,D) provides an unequivocal means to identify the pre- and postsynaptic components, with the axon terminal containing complementary (matching) images of >10 densely-packed round or hemispherical 50-nm-diameter SVs (Figs. 9C,D; lavender overlays) that are characteristic of glutamatergic and other excitatory chemical synapses. As in thin sections, the extracellular space in this cross-fractured synaptic contact (Fig. 9C-D and insets in both) is narrowed (characteristic of gap junctions). Notably, 10-nm gold beads (for Cx35) lie on the presynaptic side of the cross-fractured gap junction (*arrows*), whereas 5-nm gold beads Cx34.7 (*arrowheads*) label Cx34.7 in the postsynaptic (somatic) cytoplasm. This cross-fracture view provides an independent way of confirming the asymmetric distribution of Cx35 and Cx34.7 to pre- vs. postsynaptic hemiplaques. Overall, in FRIL matched double-replica images of non-MC mixed synapses containing a total of 100 hemiplaques, 40 of 40 (100%) presynaptic hemiplaques were labeled for Cx35 but not Cx34.7, and 60 of 60 (100%) of postsynaptic hemiplaques were labeled for Cx34.7 but not Cx35. These data include three cross-fractures, with their presynaptic sides labeled solely for Cx35 and their postsynaptic sides labeled for Cx34.7 (Figs. 9C,D)

FRIL identification of glutamate receptor clusters

Most Cx35/Cx34.7-containing gap junctions encountered to date in goldfish hindbrain were at positively-identified glutamatergic mixed synapses. In double-, triple-, and quadruple-labeled samples that included labeling for NMDAR1, distinctive clusters of 10-nm E-face particles that were immediately adjacent to gap junctions (*i.e.*, separated by 0.03-0.3 μm) were consistently immunogold-labeled by antibodies to NMDAR1 (Fig. 11A), as previously shown in goldfish (Pereda et al., 2003) and rodent glutamatergic synapses (Rash et al., 2004; Rash et al., 2005; Hamzei-Sichani et al., 2012). In samples not labeled for NMDA receptors, glutamatergic mixed synapses were nevertheless positively identified in postsynaptic views

by the presence of similar distinctive clusters of 10-nm E-face particles (yellow overlays in Figs. 7A; 10B,C; 13A-C) or clusters of 10-nm P-face pits (Fig. 7B, yellow overlay).

Morphologies of synaptic contacts

Chemical, electrical, and mixed synapses have six basic morphologies, two of which are illustrated in this report: *1)* distinct "ball-and-socket" invaginations into the postsynaptic soma or dendrite (Figs. 9; 10A; 11B; 12); *2)* flat areas that were neither invaginated nor evaginated (Fig. 12, flattened synapses distributed between the ball-and-socket synapses), *3)* small, often clublike evaginations forming dendritic spines (not shown), *4)* more complex evaginations forming thorny excrescences, some of which have gap junctions (Hamzei-Sichani et al., 2012) (thorny excrescences not seen in this study of goldfish brain), and *5)* purely electrical synapses, primarily at flattened dendro-dendritic appositions, none of which were found by our Cx35/Cx34.7-labeling strategy [but see (Kosaka, 1983; Kosaka and Hama, 1985; Fukuda and Kosaka, 2000a; Kosaka and Kosaka, 2004; Kosaka and Kosaka, 2005; Rash et al., 2005; Fukuda et al., 2006) for multiple examples]. 6) In addition, we found one small (*ca.* 50 connexons) Cx35-labeled gap junction on a single, small, *en passant*, presumably dopaminergic axon terminal (not shown). Other rare synaptic morphologies were either not labeled for either Cx35 or Cx34.7, not encountered, or not recognized in this study.

Inhibitory mixed synapses not detected by our FRIL search strategy

In FRIL searches of soma and axon hillock membranes, which are enriched in inhibitory synapses (Diamond and Huxley, 1968), no Cx35 or Cx34.7-containing gap junctions were found in an estimated 300+ putative inhibitory synapses (Fig. 12; P-face PSDs indicated by *orange overlays*), and similarly, no inhibitory mixed synapses labeled for Cx35 or Cx34.7 were encountered anywhere in the non-somatic neuropil of any brain region. The principal types of inhibitory chemical synapses, primarily GABAergic and glycinergic synapses, were identified by the presence of distinctive PSDs composed of clusters of 8-10 nm P-face particles (Legendre, 2001; Kasugai et al., 2010) (Fig. 12). Inhibitory mixed synapses are readily discriminated from excitatory (including glutamatergic) synapses, which instead, have tightly-clustered 10-nm E-face particles in their PSDs (Figs. 10B,C; 11A,B). Thus, most gap junctions found to date in goldfish brain were at identified glutamatergic synapses (55%) or at identified excitatory mixed synapses in which the neurotransmitter receptors were not seen but 50-nm-diameter round synaptic vesicles were observed in the axon terminal (14%). The remaining 31% of synapses having gap junctions were not identifiable because no presynaptic markers (synaptic vesicles) and no postsynaptic markers (E- or P-face glutamate receptor clusters) were visible, usually reflecting visualization of a labeled gap junction with little or no surrounding membrane or cytoplasm to establish context. Importantly, none (0%) were at identified inhibitory chemical synapses (see Fig. 12). Note also that the unidentified 31% of synapses with gap junctions also likely correspond to glutamatergic mixed synapses because definitive markers for glutamate receptors cannot be discerned in any presynaptic fractures, thereby eliminating between 25% and 50% of possible views from positive identification. This is because 50% of fractures are primarily presynaptic and 50% are primarily postsynaptic. Thus, *ca.* 25% of views are presynaptic P-faces and 25% are presynaptic E-faces, many of which do not also contain views with

postsynaptic markers. Likewise, many of the purely postsynaptic views do not contain sufficient area to reveal postsynaptic receptor clusters, also making some postsynaptic views unidentifiable. From the above, we conclude that Cx35 or Cx34.7-containing inhibitory mixed synapses, either GABAergic or glycinergic, either do not occur in goldfish brain, they are extremely rare, or they utilize a different connexin, such as teleost homologs of Cx45, for which we have no proven antibodies.

Gap junctions/mixed synapses in other areas of goldfish brain

By FRIL, ultrastructurally-defined, Cx35- and Cx34.7-immunogold-labeled neuronal gap junctions were found where immunofluorescence imaging had revealed discrete “puncta” (see Figs. 2-4), including in midbrain (optic tectum; Fig. 13C; and torus semicircularis, not shown), and in hindbrain (rhombomeres 2-7, shown above), and corpus cerebelli (Figs. 13A,B,D). Although it would have been excessively laborious to use FRIL to analyze all regions of goldfish brain and spinal cord (see rationale in EXPERIMENTAL PROCEDURES), Cx35 was present only in presynaptic hemiplaques and not in postsynaptic hemiplaques in all areas examined. However, in some samples that were well labeled for Cx35 in presynaptic hemiplaques, labeling of postsynaptic hemiplaques was absent (Fig. 11C, blue overlay), revealing that the particular antibody aliquot for Cx34.7 was not effective under the washing and labeling conditions employed for that sample. Thus, numerical data for presynaptic labeling by Cx35 are included, but data and conclusion from those samples ostensibly labeled for Cx34.7, including for detection and quantification of possible dendro-dendritic gap junctions, are not considered reliable and thus are not included (see next section).

Purely electrical synapses

In all Cx35-labeled samples, and in three samples that were well labeled for both Cx35 and Cx34.7 (#811 and “DRD top” and “DRD-bottom”), gold beads provided highly-visible “flags” that facilitated detection of immunogold-labeled neuronal gap junctions. However, in those samples, we did not encounter a positively-identified dendro-dendritic, purely electrical synapse. Because of the consistently high labeling efficiency for Cx35 in all samples, the lack of detection of Cx35-containing dendro-dendritic synapses using our immunogold search strategy (see EXPERIMENTAL PROCEDURES) means that dendro-dendritic synapses containing Cx35 in either hemiplaque either do not exist or they are extremely rare in the brain areas examined. However, because of weaker and inconsistent labeling for Cx34.7, we cannot eliminate the possible occurrence of homotypic Cx34.7 dendro-dendritic gap junctions; and indeed, that combination might be expected because Cx34.7 is shown above to be restricted to somatic and dendritic plasma membranes. This means that if Cx34.7 were present in either or both sides of hypothetical dendro-dendritic electrical synapses, we should have detected at least half of them, whereas none were detected. Moreover, we have not examined the inferior olive, pallium (the goldfish correlate of the hippocampus), or other regions in goldfish brain corresponding to areas in which purely electrical synapses (including dendro-dendritic synapses) have been found in mammalian brain (Baker and Llinás, 1971; Kosaka, 1983; Kosaka and Hama, 1985; Katsumaru et al., 1988; Fukuda and Kosaka, 2000a; Fukuda and Kosaka, 2000b; Kosaka and Kosaka, 2004; Kosaka and Kosaka, 2005; Fukuda et al., 2006; Hoge et al., 2011)]. Thus, the

possibility of dendro-dendritic electrical synapses in goldfish brain remains largely unexplored by FRIL. Additional samples with improved Cx34.7 labeling will be required to determine if homotypic Cx34.7 forms both sides of any dendro-dendritic gap junction. Finally, we note that dendro-dendritic gap junctions and/or gap junctions at GABAergic synapses could be formed from an entirely different connexin – for example homologs of Cx45 – and if so, they would not have been detected in this study of Cx35/Cx34.7-containing gap junctions.

Heterotypic gap junctions in goldfish brain are homomeric

Of >700 FRIL, DR-SDS-FRL, and DR-FRIL images of immunogold –labeled gap junctions in adult goldfish brain found to date, no examples were found of mixed Cx35/Cx34.7 in the same hemiplaque of any gap junction (Figs. 7, 8, 11, 13). This clear segregation of labeling reveals that all presynaptic connexons in gap junctions labeled for Cx35 and or Cx34.7 are homomeric with respect to Cx35 (and its orthologs) and that all postsynaptic connexon hemichannels are homomeric with respect to Cx34.7 (and its orthologs; see DISCUSSION). This also means that the gap junctions of glutamatergic mixed synapses, whether forming homologous or heterologous couplings between similar or dissimilar neurons in goldfish brain, are heterotypic, providing inherently asymmetric coupling in all brain regions examined.

Discussion

Cx35/Cx34.7-containing gap junctions are exclusively heterotypic

Previously, gap junctions in teleost species were found and extensively studied in three primary locations – LMCE/M-cell mixed synapses (Tuttle et al., 1986; Nakajima et al., 1987; Lin and Faber, 1988; Pereda et al., 2003), at electrosensory and electromotor neurons of weakly electric fish (Bennett et al., 1963; Pappas and Bennett, 1966; Bennett et al., 1967a; Kriebel et al., 1969; Payton et al., 1969; Maler et al., 1981; Carr et al., 1986; Mathieson et al., 1987), and in retina (Witkovsky et al., 1974; Naka and Christensen, 1981; Kurz-Isler and Wolburg, 1986; Marc et al., 1988; Wolburg and Rohlmann, 1995; O'Brien et al., 2004; Kothmann et al., 2007; Arai et al., 2010), the latter of which has the greatest variety of synaptic configurations involving gap junctions, and which we do not address here. This prior focus of studies on a few CNS regions potentially left the impression that gap junctions are otherwise rare in the teleost CNS. However, here we used confocal immunofluorescence microscopy, FRIL, and matched double-replica FRIL to show: 1) that immunofluorescent puncta and ultrastructurally-identified Cx34.7/Cx35-containing neuronal gap junctions are abundant and widespread in the goldfish brain, 2) that in the regions examined, Cx35/Cx34.7-containing gap junctions are primarily at glutamatergic mixed synapses (Fig. 14), 3) that Cx35 immunoreactivity is exclusively in presynaptic hemiplaques at these mixed synapses, and 4) that Cx34.7 immunoreactivity is exclusively in postsynaptic hemiplaques at those same mixed synapses, including in matched mirror-image complements. We conclude that symmetric distribution of either or both of these two connexins must be rare in the regions examined, as no symmetric gap junctions were found among the >700 gap junctions detected by these labeling methods. Moreover, 5) although hundreds of presumptive GABAergic and glycinergic synapses (identified by their

distinctive clusters of 10-nm P-face particles) were found, often intermixed with glutamatergic synapses, none of the inhibitory synapses had Cx35/Cx34.7-containing gap junctions on any neuron that we encountered in any FRIL or DR-FRIL replicas, indicating either that inhibitory mixed synapses are rare or non-existent in goldfish brain or that they are formed by different connexins (Fig. 14 bottom). And, as qualified below, 6) our FRIL approaches have not yet revealed any Cx35-containing gap junctions forming purely electrical synapses (Fig. 14, middle). Additional experiments will be required to determine whether such gap junctions are formed by homotypic Cx34.7, by homologs of Cx45, or by some other connexin.

Although antibody labeling was weaker and less consistent for Cx34.7 than for Cx35, occasionally failing entirely (Fig. 11C), in FRIL samples where labeling for Cx34.7 was robust, labeling for Cx34.7 was exclusively postsynaptic (Figs. 8, 9). With no postsynaptic labeling for Cx35 and with approximately equal numbers of connexons on both sides of each gap junction [except for continuing insertion of a few unpaired connexins (Flores et al., 2012)], we suggest that both Cx34.7 and Cx35 must be equally present at each gap junction at glutamatergic mixed synapses, with exclusively presynaptic Cx35 coupling with exclusively postsynaptic Cx34.7.

Dendro-dendritic electrical synapses not detected by FRIL labeling for Cx35

Curiously, our strategy of searching for immunogold rather than gap junctions revealed no examples of dendro-dendritic electrical synapses, even though dendro-dendritic gap junctions have been described in several regions of teleost brain (Pappas and Bennett, 1966; Bennett et al., 1967a; Bennett et al., 1967b; Bennett et al., 1967c; Korn et al., 1977; Sotelo and Korn, 1978; Castelló et al., 1998), and many have been found in mammalian CNS (Bennett and Zukin, 2004; Connors and Long, 2004). We advance several potential explanations for these contrasting observations. First, this may represent a major species difference, such that dendro-dendritic, purely electrical synapses in goldfish may be relatively rare compared with dendro-dendritic synapses in higher vertebrates, some of which contain Cx36 (Fukuda et al., 2006), the mammalian ortholog of Cx35 and Cx34.7. Second, purely electrical synapses in goldfish may be composed of yet additional neuronal connexins – for example orthologs of mammalian Cx45 – and hence not detected by the antibodies against Cx34.7 and Cx35 used here. Third, purely electrical synapses in goldfish may be restricted to CNS regions that we have not searched by FRIL. And fourth, labeling for Cx34.7 was weak or non-existent in some samples, precluding our detection of possible homotypic Cx34.7-containing purely electrical synapses in those samples.

Which connexins occur at dendro-dendritic electrical synapses?

Based on the above FRIL data, dendro-dendritic electrical synapses cannot be composed of Cx35 alone, nor can they be composed of mixed Cx34.7+Cx35 on both sides of dendritic appositions (*i.e.*, as bi-homotypic coupling) because our Cx35 search strategy revealed no dendritic gap junctions containing Cx35 alone or in combination with Cx34.7. However, our Cx34.7 search strategy might not have detected dendro-dendritic gap junctions composed solely of Cx34.7 in both apposed dendrites (*i.e.*, homotypic Cx34.7**:**Cx34.7 coupling). But if such gap junctions occur, they would have to occur only in those replicas of goldfish

forebrain and midbrain in which labeling for Cx34.7 was weak or non-existent, because dendro-dendritic gap junctions were not detected in brainstem slices well-labeled for both Cx35 and Cx34.7 (see Figs. 8, 9 for strong labeling of both connexins). Finally, our data allow for dendro-dendritic gap junctions composed of some other connexin or connexins (*e.g.,* homologs of Cx45). Additional experiments using new antibodies to other neuronal connexins will be required to determine which from the above possibilities is/are correct.

Heterologous coupling via heterotypic gap junctions

In teleost hindbrain and spinal cord, most gap junctions represent heterologous couplings of axon terminals onto somata and "somatic dendrites" of unlike neurons (Diamond and Huxley, 1968), including sensory neurons coupled to motor neurons (this report) and interneurons coupled to principal or projection neurons (Maler et al., 1981; Serrano-Vélez et al., 2014). This widespread heterologous coupling is in contrast with the often, though not exclusive, homologous coupling found at dendro-dendritic, presumably "purely electrical" synapses in mammalian CNS (Kosaka, 1983; Kosaka and Hama, 1985; Fukuda and Kosaka, 2000a; Kosaka and Kosaka, 2004; Kosaka and Kosaka, 2005; Fukuda et al., 2006). In view of the above, it is interesting to consider the possibility that the heterologous coupling between neurons seen so widely in goldfish hindbrain and spinal cord requires an asymmetric heterotypic configuration of connexins, whereas abundant homologous coupling at purely electrical synapse between similar neuronal classes in mammals may be a consequence of a single connexin being expressed in both sides of gap junctions in these neurons. While there is evidence for heterologous coupling (*i.e.,* between dissimilar neuronal classes) at a few sites in mammalian CNS, involving both mixed synapses (Korn et al., 1973; Nagy, 2012; Nagy et al., 2013; Bautista et al., 2014) and presumptive purely electrical synapses (Apostolides and Trussell, 2013), it is not yet clear whether the gap junctions at these heterologous couplings consist of homotypic or heterotypic junctions, and if homotypic, whether they have asymmetric molecular modifications of Cx36.

Glutamatergic mixed synapses are abundant in teleost and rodent CNS

We have also demonstrated the abundance of glutamatergic mixed synapses composed of Cx35 and/or Cx34.7 in brainstem and spinal cord of other teleost species (Serrano-Vélez et al., 2014; Yao et al., 2014). Although only a few areas of mammalian CNS have been similarly investigated, neurons in rodent spinal cord have relatively abundant mixed synapses (Rash et al., 1996), and those in mesencephalic trigeminal nucleus and in spinal cord were recently identified as vGlut1-positive (*i.e.,* glutamatergic) mixed synapses (Nagy et al., 2013; Bautista et al., 2014). Moreover, we and others have described glutamatergic mixed synapses in other CNS regions, including lateral vestibular nucleus, hippocampus, retina, and olfactory bulb (Korn et al., 1973; Rash et al., 2005; Kamasawa et al., 2006; Hamzei-Sichani et al., 2012; Nagy, 2012; Kothmann et al., 2012; Nagy et al., 2013). Thus, similar to what has been shown in weakly electric fish (Maler et al., 1981; Carr et al., 1986; Mathieson et al., 1987), in spinal cord of mosquitofish (Serrano-Vélez et al., 2014), and is now shown throughout goldfish hindbrain, glutamatergic mixed synapses in mammalian systems appear to represent an important subset of excitatory synapses.

Connexins expressed in teleost species

In contrast to the single primary neuronal connexin protein in mammals (*i.e.*, Cx36; designating a 36 kDa protein) (Condorelli et al., 1998), a whole-genome duplication event occurred in stem teleosts (Amores et al., 1998; Eastman et al., 2006), allowing for molecular divergence of the amino acid sequences of duplicated homologs (McLysaght et al., 2002). The superclass *Osteichthyes* consists of two classes of bony fish: The “lobe-finned” fishes (*Sarcopterygii*), today consisting of coelacanths and lungfish but formerly including ancestors of all tetrapod species (amphibia, reptiles, birds and mammals), and these retained the ancestral vertebrate genome (Sato and Nishida, 2010). The other major branch of the “ray-finned” fishes (*Actinopterygii*) that led to most teleost species (but excluding sturgeons, bowfins, and gars), experienced a second whole-genome duplication (Sato and Nishida, 2010), which allowed divergence of duplicated genes (Christie and Jelinek, 1993; McLysaght et al., 2002), resulting in four orthologs of tetrapod Cx36 (*i.e.*, Cx34.1, Cx34.7, Cx35, Cx35.5; Adam Miller, personal communication; John O'Brien, unpublished data). Although detailed immunocytochemical characterization of the four Cx36 orthologs is beyond the scope of this report, it is clear from the current DR-FRIL data that Cx34.7 immunoreactivity, whether for one or both Cx34.7 orthologs, is detected only postsynaptically, whereas Cx35 immunoreactivity, whether for one or both Cx35 orthologs, is detected only presynaptically.

Early ultrastructural studies described a wide distribution of neuronal gap junctions in fish, and it is likely that Cx35 and Cx34.7 are expressed in many of those, including ultrastructurally-identified mixed synapses in various CNS regions that utilize a variety of complex brain circuitries in various species of fish (Ito, 1974; Bennett et al., 1978; Sotelo and Korn, 1978; Bennett and Goodenough, 1978; Maler et al., 1981; Kosaka and Hama, 1982; Uchiyama and Ito, 1984; Hackett and Buchheim, 1984; Carr et al., 1986; Mathieson et al., 1987; Zupanc, 1991; Castello et al., 1998). With antibodies now available for Cx34.7 and Cx35 (O'Brien et al., 1996; O'Brien et al., 1998; O'Brien et al., 2004), the separate localization of immunoreactivity for these two connexins has not yet been examined by FRIL in most major structures of teleost brain, but we have provided a brief confocal microscopic immunofluorescence overview (Figs. 2-4) of their composite distribution using an antibody that detects both of these connexin orthologs. It is only by extrapolation from the present FRIL results and from parallel fluorescence studies of LMCE/M-cell contacts that we infer the probable co-localization of these two connexin into separate apposed hemiplaques at those abundant sites of immunofluorescence punctate labeling thorughout goldfish brain.

Sorting and trafficking of heterotypic connexins

Our observations regarding asymmetric distribution of Cx35 *vs.* Cx34.7 at glutamatergic mixed synapses lead to three alternative hypotheses: 1) that the observed asymmetry of connexin expression is based on sensory neurons expressing only Cx35, whereas Mauthner cells and other projection neurons express only Cx34.7; 2) that both Cx35 and Cx34.7 are expressed by sensory neurons, motor neurons, and interneurons, but with Cx35 sorted and transported to plasma membranes of axon terminals, whereas Cx34.7 is sorted and inserted only into plasma membranes of somata and dendrites; or 3) that Cx35 and Cx34.7

specifically associate with protein complexes characteristic of pre- *vs.* post-synaptic elements, respectively, of glutamatergic synapses, resulting in the asymmetric distribution of connexins shown here. It is of note that in these fish orthologs of Cx36, differential amino acid alterations occur primarily in the cytoplasmic loops (O'Brien et al., 1998), but minor differences also occur in the carboxyl terminal and extracellular loop domains. It is possible that these differences influence protein-protein interactions that direct trafficking, which may allow a single neuron to synthesize both connexins, but to differentially target Cx35 to its axon terminal(s) and Cx34.7 to its somatic and dendritic plasma membranes. In cone photoreceptors of bass retina, Cx35 and Cx34.7 are expressed together but are targeted to different electrical synapses in the axon terminals (O'Brien et al., 2004), indicating that targeting of these connexins may be exquisitely specific. As further precedent for differential subcellular targeting, differential targeting of connexins has been observed in oligodendrocytes, where Cx32 but not Cx47 is present in internal myelin layers, whereas both Cx32 and Cx47 are present in the outermost layer of myelin (Li et al., 2008).

Molecular asymmetry and its functional consequences

Rectification of electrical transmission is generally associated with heterotypic gap junction channels. Our recent findings indicate that asymmetric distribution of Cx34.7 *vs.* Cx35 at LMCE/M-cell mixed synapses is associated with electrical rectification (Rash et al 2013). The present results showing a similar asymmetric localization of these two connexins at gap junctions of mixed synapses throughout goldfish midbrain and hindbrain suggest that rectification may occur in other regions of teleost CNS. We hypothesize that asymmetric gap junctions composed of apposing Cx34.7/Cx35 at glutamatergic mixed synapses is one means of providing the potential for electrical rectification in all regions of the teleost CNS wherein they occur. Indeed, rectification in teleosts was observed many years ago at giant axon/motor neuron electrical synapses in hatchetfish (Auerbach and Bennett, 1969), but the molecular basis conferring rectifying properties at these gap junctions remains unknown, and the identity of their connexins is not yet established. The physiological relevance of rectification has been discussed in the context of facilitated synaptic transmission via lateral excitation (Pereda et al., 2004) and in making electrical transmission bidirectional under conditions in which the geometry of the coupled neuronal processes is unfavorable for transmission in one of the directions (Rash et al., 2013). However, other complex interactions are possible, particularly if the direction and strength of rectification is dynamically regulated by neuronal activity (Trenholm et al., 2013; Lefler et al., 2014).

The widespread distribution of heterotypic gap junctions suggests that rectification might not be the only functional advantage of this asymmetric synaptic configuration. Moreover, this widespread distribution of heterotypic gap junctions throughout the teleost CNS [current results, plus (Rash et al., 2013; Serrano-Vélez et al., 2014; Yao et al., 2014)] implies that pre- *vs.* postsynaptic asymmetry at electrical synapses evolved early in the chordate lineage and has been maintained for >300,000,000 years. We suggest that the selective advantages of such asymmetry in the molecular composition of the pre- and postsynaptic sites at electrical synapses are unlikely to have been abandoned in higher vertebrates, including mammals. Asymmetries might not solely involve differences in the connexin composition of the contributing hemichannels, but also could be based on differences in the state of

phosphorylation of Cx36 on opposite sides of a gap junction (Rash et al., 2007) or could reflect differences in the complement of scaffolding and regulatory proteins of homotypic gap junctions, such as those associated with Cx36 (Li et al., 2004; Ciolofan et al., 2006; Lynn et al., 2012; Li et al., 2012). Therefore, we note that in similarity to pre- and postsynaptic sites at chemical synapses, the molecular composition of each side at neuronal gap junction can be different, potentially endowing gap junctions/electrical synapses with complex functional properties.

Acknowledgments

Funded in part by grants from NIH (R01NS044395 and S10RR028936 to JER; R01EY012857 to JOB; and R01DC011099 to AP) and by the Canadian Institute for Health Research (CIHR) to JIN. Electron microscopy conducted in the Microscope Imaging Network at Colorado State University. We thank B. McLean for excellent technical assistance, D. Tsao and S. Wang for assistance with counts of immunofluorescence puncta, and Jordan Hickman for assistance quantifying FRIL images. We also thank Adam Miller for reading the manuscript and allowing us to refer to his unpublished data.

References

Amores A, Force A, Yan YL, Joly L, Amemiya C, Fritz A, Ho RK, Langeland J, Prince V, Wang YL, Westerfield M, Postlethwait JH. Zebrafish hox clusters and vertebrate genome evolution. Science. 1998; 282:1711–1714. [PubMed: 9831563]

Apostolides PF, Trussell LO. Regulation of interneuron excitability by gap junction coupling with principal cells. Nature Neurosci. 2013; 16:1764–1772. [PubMed: 24185427]

Arai I, Tanaka M, Tachibana M. Active roles of electrically coupled bipolar cell network in the adult retina. J Neurosci. 2010; 30:9260–9270. [PubMed: 20610761]

Auerbach AA, Bennett MVL. A rectifying electrotonic synapse in the central nervous system of a vertebrate. J Gen Phys. 1969; 53:211–237.

Baker R, Llinás R. Electrotonic coupling between neurones in the rat mesencephalic nucleus. J Physiol. 1971; 212:45–63. [PubMed: 5545184]

Bartelmez GW. Mauthner's cell and the nucleus motorius tegmenti. J Comp Neurol. 1915; 25:87–128.

Bautista W, McCrea DA, Nagy JI. Connexin36 identified at morphologically mixed chemical/electrical synapses on trigeminal motoneurons and at primary afferent terminals on spinal cord neurons in adult mouse and rat. Neuroscience. 2014; 263:159–180. [PubMed: 24406437]

Bennett MV, Pappas GD, Gimenez M, Nakajima Y. Physiology and ultrastructure of electrotonic junctions. IV. Medullary electromotor nuclei in gymnotid fish. J Neurophysiol. 1967a; 30:236–300. [PubMed: 6045196]

Bennett MVL, Aljure E, Nakajima Y, Pappas GD. Electrotonic junctions between teleost spinal neurons: Electrophysiology and ultrastructure. Science. 1963; 141:262–264. [PubMed: 13967485]

Bennett MVL, Goodenough DA. Gap junctions, electrotonic coupling and intercellular communication. Neuroscie Res Prog Bulletin. 1978; 16:373–486.

Bennett MVL, Pappas GD, Aljure E, Nakajima Y. Physiology and ultrastructure of electrotonic junctions. II. Spinal and medullary electromotor nuclei in mormyrid fish. J Neurophysiol. 1967b; 30:180–208. [PubMed: 4167209]

Bennett MVL, Sandri C, Akert K. Neuronal gap junctions and morphologically mixed synapses in the spinal cord of a teleost, *Sternarchus albifrons*(gymnotoidei). Brain Res. 1978; 143:43–60. [PubMed: 630403]

Bennett MVL, Zukin RS. Electrical coupling and neuronal synchronization in the mammalian brain. Neuron. 2004; 41:495–511. [PubMed: 14980200]

Bennett MV, Nakajima Y, Pappas GD. Physiology and ultrastructure of electrotonic junctions. I. Supramedullary neurons. J Neurophysiol. 1967c; 30:l–179.

Bodian D. The structure of the vertebrate synapse. A study of the axon endings on Mauthner's cell and neighboring centers in the goldfish. J Comp Neurol. 1937; 68:117–160.

Branton D, Bullivant S, Gilula NB, Karnovsky MJ, Moor H, Northcote DH, Packer L, Satir B, Satir P, Speth V, Staehelin LA, Steere RL, Weinstein RS. Freeze-etching nomenclature. Science. 1975; 190:54–56. [PubMed: 1166299]

Carr CE, Maler L, Taylor B. A time-comparison circuit in the electric fish midbrain. II. Functional morphology. J Neurosci. 1986; 6:1372–1383. [PubMed: 3711985]

Castello ME, Caputi A, Trujillo-Cenóz O. Structural and functional aspects of the fast electrosensory pathway in the electrosensory lateral line lobe of the pulse fish *Gymnotus carapo*. J Comp Neurol. 1998; 401:549–563. [PubMed: 9826277]

Castelló ME, Caputi A, Trujillo-Cenóz O. Structural and functional aspects of the fast electrosensory pathway in the electrosensory lateral line lobe of the pulse fish Gymnotus carapo. J Comp Neurol. 1998; 401:549–563. [PubMed: 9826277]

Chandler DE, Heuser J. Membrane fusion during secretion: cortical granule exocytosis in sea urchin eggs as studied by quick-freezing and freeze-fracture. J Cell Biol. 1979; 83:91–108. [PubMed: 574515]

Christie JM, Jelinek HF. Dye-coupling among neurons of the rat locus coeruleus during postnatal development. Neuroscience. 1993; 56:129–137. [PubMed: 7694183]

Ciolofan C, Li X, Olson C, Kamasawa N, Yasumura T, Morita M, Rash JE, Nagy JI. Association of connexin36 and ZO-1 with ZO-2 and the MsY3 transcription factor ZO-1 associated nucleic acid-binding protein (ZONAB) in mouse retina. Neuroscience. 2006; 140:433–451. [PubMed: 16650609]

Cohen SA, Pumplin DW. Clusters of intramembrane particles associated with binding sites for alpha-bungarotoxin in cultured chick myotubes. J Cell Biol. 1979; 82:494–516. [PubMed: 479313]

Condorelli DF, Parenti R, Spinella F, Salinaro AT, Belluardo N, Cardile V, Cicirata F. Cloning of a new gap junction gene (Cx36) highly expressed in mammalian brain neurons. Eur J Neurosci. 1998; 10:1202–1208. [PubMed: 9753189]

Connors BW, Long MA. Electrical synapses in the mammalian brain. Ann Rev Neurosci. 2004; 27:393–418. [PubMed: 15217338]

Diamond J, Huxley AF. The activation and distribution of GABA and L-glutamate receptors on goldfish Mauthner neurones: an analysis of dendritic remote inhibition. J Physiol. 1968; 194:669–723. [PubMed: 5636994]

Dinchuk JE, Johnson TJA, Rash JE. Postreplication labeling of E-leaflet molecules: Membrane immunoglobulins localized in sectioned labeled replicas examined by TEM and HVEM. J Electron Microsc Tech. 1987; 7:1–16. [PubMed: 2464678]

Eastman SD, Chen THP, Falk MM, Mendelson TC, Iovine M. Phylogenetic analysis of three complete gap junction gene families reveals lineage-specific duplications and highly supported gene classes. Genomics. 2006; 87:265–274. [PubMed: 16337772]

Eaton RC, Farley RD, Kimmel CB, Schabtach E. Functional development in the Mauthner cell system of embryos and larvae of the zebra fish. J Neurobiol. 1977; 8:151–172. [PubMed: 856948]

Flores CE, Nannapaneni S, Davidson KGV, Yasumura T, Bennett MVL, Rash JE, Pereda AE. Trafficking of gap junction channels at a vertebrate electrical synapse in vivo. Proc Natl Acad Sci (USA). 2012; 109:E573–E582. [PubMed: 22323580]

Fujimoto K. Freeze-fracture replica electron microscopy combined with SDS digestion for cytochemical labeling of integral membrane proteins. Application to the immunogold labeling of intercellular junctional complexes. J Cell Sci. 1995; 108:3443–3449. [PubMed: 8586656]

Fujimoto K. SDS-digested freeze-fracture replica labeling electron microscopy to study the two-dimensional distribution of integral membrane proteins and phospholipids in biomembranes: practical procedure, interpretation and application. Histochem Cell Biol. 1997; 107:87–96. [PubMed: 9062793]

Fukuda T, Kosaka T. Gap junctions linking the dendritic network of GABAergic interneurons in the hippocampus. J Neurosci. 2000a; 20:1519–1528. [PubMed: 10662841]

Fukuda T, Kosaka T, Singer W, Galuske RAW. Gap junctions among dendrites of cortical GABAergic neurons establish a dense and widespread intercolumnar network. J Neurosci. 2006; 26:3434–3443. [PubMed: 16571750]

Fukuda T, Kosaka T. The dual network of GABAergic interneurons linked by both chemical and electrical synapses: a possible infrastructure of the cerebral cortex. Neurosci Res. 2000b; 38:123–130. [PubMed: 11000438]

Furshpan EJ. “Electrical transmission” at an excitatory synapse in a vertebrate brain. Science. 1964; 144:878–880. [PubMed: 14149407]

Hackett JT, Buchheim A. Ultrastructural correlates of electrical-chemical synaptic transmission in goldfish cranial motor nuclei. J Comp Neurol. 1984; 224:425–436. [PubMed: 6325513]

Haggis GH. Electron microscope replicas from the surface of a fracture through frozen cells. J Biophys Biochem Cytol. 1961; 9:841–852. [PubMed: 13710524]

Hamzei-Sichani F, Davidson KGV, Yasumura T, Janssen WGM, Wearne SL, Hof PR, Traub RD, Gutierrez R, Ottersen OP, Rash JE. Mixed electrical-chemical synapses in adult rat hippocampus are primarily glutamatergic and coupled by connexin-36. Front Neuroanat. 2012; 6:1–26. [PubMed: 22291620]

Hanneman E, Trevarrow B, Metcalfe WK, Kimmel CB, Westerfield M. Segmental pattern of development of the hindbrain and spinal cord of the zebrafish embryo. Development. 1988; 103:49–58. [PubMed: 3197633]

Harris KM, Landis DMD. Membrane structure at synaptic junctions in area CA1 of the rat hippocampus. Neuroscience. 1986; 19:857–872. [PubMed: 3796819]

Hoge G, Davidson KG, Yasumura T, Castillo PE, Rash JE, Pereda AE. The extent and strength of electrical coupling between inferior olivary neurons is heterogeneous. J Neurophysiol. 2011; 105:1089–1101. [PubMed: 21177999]

Ito H. Fine structure of the torus semicircularis of some teleosts. J Morph. 1974; 142:137–152. [PubMed: 4811245]

Kamasawa N, Furman CS, Davidson KGV, Sampson JA, Magnie AR, Gebhardt B, Kamasawa M, Morita M, Yasumura T, Pieper M, Zumbrunnen JR, Pickard GE, Nagy JI, Rash JE. Abundance and ultrastructural diversity of neuronal gap junctions in the OFF and ON sublaminae of the inner plexiform layer of rat and mouse retina. Neuroscience. 2006; 142:1093–1117. [PubMed: 17010526]

Kasugai Y, Swinny JD, Roberts JD, Dalezios Y, Fukazawa Y, Sieghart W, Shigemoto R, Somogyi P. Quantitative localisation of synaptic and extrasynaptic $GABA_A$ receptor subunits on hippocampal pyramidal cells by freeze-fracture replica immunolabelling. Eur J Neurosci. 2010; 32:1868–1888. [PubMed: 21073549]

Katsumaru H, Kosaka T, Heizmann CW, Hama K. Gap junctions on GABAergic neurons containing the calcium-binding protein parvalbumin in the rat hippocampus (CA1 region). Exp Brain Res. 1988; 72:363–370. [PubMed: 3066635]

Korn H, Sotelo C, Bennett MVL. The lateral vestibular nucleus of the toadfish *Opsanus tau*: Ultrastructural and electrophysiological observations with special reference to electrotonic transmission. Neuroscience. 1977; 2:851–884.

Korn H, Sotelo C, Crepel F. Electrotonic coupling between neurons in rat lateral vestibular nucleus. Exp Brain Res. 1973; 16:255–275. [PubMed: 4346867]

Kosaka T. Gap junctions between non-pyramidal cell dendrites in the rat hippocampus (CA1 and CA3 regions). Brain Res. 1983; 271:157–161. [PubMed: 6883113]

Kosaka T, Hama K. Gap junctions between non-pyramidal cell dendrites in the rat hippocampus (CA1 and CA3 regions): a combined golgi-electron microscopy study. J Comp Neurol. 1985; 231:150–161. [PubMed: 3968232]

Kosaka T, Hama K. Structure of the mitral cell in the olfactory bulb of the goldfish (Carassius auratus). J Comp Neurol. 1982; 212:365–384. [PubMed: 7161415]

Kosaka T, Kosaka K. Neuronal gap junctions between intraglomerular mitral/tufted cell dendrites in the mouse main olfactory bulb. Neurosci Res. 2004; 49:373–378. [PubMed: 15236862]

Kosaka T, Kosaka K. Intraglomerular dendritic link connected by gap junctions and chemical synapses in the mouse main olfactory bulb: Electron microscopic serial section analyses. Neuroscience. 2005; 131:611–625. [PubMed: 15730867]

Kothmann WW, Li X, Burr GS, O'Brien J. Connexin 35/36 is phosphorylated at regulatory sites in the retina. J Neuroscience. 2007; 24:363–375.

Kothmann WW, Trexler EB, Whitaker CM, Li W, Massey SC, O'Brien J. Nonsynaptic NMDA receptors mediate activity-dependent plasticity of gap junctional coupling in the AII amacrine cell network. J Neurosci. 2012; 32:6747–6759. [PubMed: 22593045]

Kriebel ME, Bennett MVL, Waxman SG, Pappas GD. Oculomotor neurons in fish: electrotonic coupling and multiple sites of impulse initiation. Science. 1969; 166:520–524. [PubMed: 4309628]

Kurz-Isler G, Wolburg H. Gap junctions between horizontal cells in the cyprinid fish alter rapidly their structure during light and dark adaptation. Neuro Lett. 1986; 67:7–12.

Landis DMD, Reese TS. Differences in membrane structure between excitatory and inhibitory synapses in the cerebellar cortex. J Comp Neurol. 1974; 155:93–126. [PubMed: 4836065]

Landis DMD, Reese TS, Raviola E. Differences in membrane structure between excitatory and inhibitory components of the reciprocal synapse in the olfactory bulb. J Comp Neurol. 1974; 155:67–92. [PubMed: 4836064]

Lee RKK, Eaton RC, Zottoli SJ. Segmental arrangement of reticulospinal neurons in the goldfish hindbrain. J Comp Neurol. 1993; 329:539–556. [PubMed: 8454739]

Lefler Y, Yarom Y, Uusisaari MY. Cerebellar inhibitory input to the inferior olive decreases electrical coupling and blocks subthreshold oscillations. Neuron. 2014; 81:1389–1400. [PubMed: 24656256]

Legendre P. The glycinergic inhibitory synapse. Cell Mol Life Sci CMLS. 2001; 58:760–793.

Li X, Kamasawa N, Ciolofan C, Olson CO, Lu S, Davidson KGV, Yasumura T, Shigemoto R, Rash JE, Nagy JI. Connexin45-containing neuronal gap junctions in rodent retina also contain connexin36 in both apposing hemiplaques, forming bi-homotypic gap junctions, with scaffolding contributed by zonula occludens-1. J Neurosci. 2008; 28:9769–9789. [PubMed: 18815262]

Li X, Lynn BD, Nagy JI. The effector and scaffolding proteins AF6 and MUPP1 interact with connexin36 and localize at gap junctions that form electrical synapses in rodent brain. Europ J Neurosci. 2012; 35:166–181.

Li X, Olson C, Lu S, Kamasawa N, Yasumura T, Rash JE, Nagy JI. Neuronal connexin36 association with zonula occludens-1 protein (ZO-1) in mouse brain and interaction with the first PDZ domain of ZO-1. Eur J Neurosci. 2004; 19:2132–2146. [PubMed: 15090040]

Lin JW, Faber DS. Synaptic transmission mediated by single Club Endings on the goldfish Mauthner cell. I. Characteristics of electrotonic and chemical postsynaptic potentials. J Neurosci. 1988; 8:1302–1312. [PubMed: 2833580]

Lynn BD, Li X, Nagy JI. Under construction: Building the macromolecular superstructure and signaling components of an electrical synapse. J Membr Biol. 2012; 245:303–317. [PubMed: 22722764]

Maler L, Sas EKB, Rogers J. The cytology of the posterior lateral line lobe of high-frequency weakly electric fish (gymnotidae): Dendritic differentiation and synaptic specificity in a simple cortex. J Comp Neurol. 1981; 195:87–139. [PubMed: 7204653]

Marc RE, Liu WL, Muller JF. Gap junctions in the inner plexiform layer of the goldfish retina. Vision Res. 1988; 28:9–24. [PubMed: 3414003]

Masugi-Tokita M, Shigemoto R. High-resolution quantitative visualization of glutamate and GABA receptors at central synapses. Cur Opinion Neurobiol. 2007; 17:387–393.

Mathieson WB, Heiligenberg W, Maler L. Ultrastructural studies of physiologically identified electrosensory afferent synapses in the gymnotiform fish, *Eigenmannia*. J Comp Neurol. 1987; 255:526–537. [PubMed: 3819029]

McLysaght A, Hokamp K, Wolfe KH. Extensive genomic duplication during early chordate evolution. Nat Genet. 2002; 31:200–204. [PubMed: 12032567]

Metcalfe WK, Mendelson B, Kimmel CB. Segmental homologies among reticulospinal neurons in the hindbrain of the zebrafish larva. J Comp Neurol. 1986; 251:147–159. [PubMed: 3782495]

Nagy JI. Evidence for connexin36 localization at hippocampal mossy fiber terminals suggesting mixed chemical/electrical transmission by granule cells. Brain Res. 2012; 1487:107–122. [PubMed: 22771400]

Nagy JI, Bautista W, Blakley B, Rash JE. Morphologically mixed chemical-electrical synapses formed by primary afferents in rodent vestibular nuclei as revealed by immunofluorescence detection of

connexin36 and vesicular glutamate transporter-1. Neuroscience. 2013; 252:468–488. [PubMed: 23912039]

Naka KI, Christensen BN. Direct electrical connections between transient amacrine cells in the catfish retina. Science. 1981; 214:462–464. [PubMed: 7291987]

Nakajima Y, Tuttle R, Masuko S, Betz H, Pfeiffer F. Synapses on the Mauthner cell of the goldfish: Thin section, freeze-fracture, and immunocytochemical studies. J Electron Microsc Tech. 1987; 6:143–153.

O'Brien J, Al-Ubaidi MR, Ripps H. Connexin35: a gap junctional protein expressed preferentially in the skate retina. Mol Biol Cell. 1996; 7:233–243. [PubMed: 8688555]

O'Brien J, Bruzzone R, White TW, Al-Ubaidi MR, Ripps H. Cloning and expression of two related connexins from the perch retina define distinct subgroups of the connexin family. J Neurosci. 1998; 18:7625–7637. [PubMed: 9742134]

O'Brien J, Nguyen HB, Mills SL. Cone photoreceptors in bass retina use two connexins to mediate electrical coupling. J Neurosci. 2004; 24:5632–5642. [PubMed: 15201336]

Oh S, Rubin JB, Bennett MVL, Verselis VK, Bargiello TA. Molecular Determinants of Electrical Rectification of Single Channel Conductance in Gap Junctions Formed by Connexins 26 and 32. J General Physiology. 1999; 114:339–364.

Palacios-Prado N, Huetteroth W, Pereda AE. Hemichannel composition and electrical synaptic transmission: molecular diversity and its implications for electrical rectification. Front Cell Neurosci. 2014; 8/324:1–13.

Pappas GD, Bennett MVL. Specialized junctions involved in electrical transmission between neurons. Ann N Y Acad Sci. 1966; 166:495–508. [PubMed: 5229811]

Payton BW, Bennett MVL, Pappas GD. Permeability and structure of junctional membranes at an electrotonic synapse. Science. 1969; 166:1641. [PubMed: 5360587]

Peracchia C. Low resistance junctions in crayfish. I. Two arrays of globules in junctional membranes. J Cell Biol. 1973a; 57:54–65. [PubMed: 4120610]

Peracchia C. Low resistance junctions in crayfish. II. Structural details and further evidence for intercellular channels by freeze-fracture and negative staining. J Cell Biol. 1973b; 57:66–76. [PubMed: 4120611]

Pereda A, O'Brien J, Nagy JI, Bukauskas F, Davidson KGV, Kamasawa N, Yasumura T, Rash JE. Connexin35 mediates electrical transmission at mixed synapses on Mauthner cells. J Neurosci. 2003; 23:7489–7503. [PubMed: 12930787]

Pereda A, Rash JE, Nagy JI, Bennett MVL. Dynamics of electrical transmission at club endings on the Mauthner cells. Brain Res Brain Res Rev. 2004; 47:227–244. [PubMed: 15572174]

Peters, A. The Fine Structure of the Aging Brain. 2014. http://www.bu.edu/agingbrain/chapter-9-synapses/

Peters, A.; Palay, SL.; Webster, HD. The Fine Structure of the Nervous System Neurons and Their Supporting Cells. New York: Oxford University Press; 1991.

Pfenninger K, Akert K, Moor H, Sandri C. The fine structure of freeze-fractured presynaptic membranes. J Neurocytol. 1972; 1:129–149. [PubMed: 4358835]

Rash JE, Curti S, Vanderpool KG, Kamasawa N, Nannapaneni S, Palacios-Prado N, Flores CE, Yasumura T, O'Brien J, Lynn BD, Bukauskas FF, Nagy JI, Pereda AE. Molecular and functional asymmetry at a vertebrate electrical synapse. Neuron. 2013; 79:957–969. [PubMed: 24012008]

Rash JE, Davidson KGV, Kamasawa N, Yasumura T, Kamasawa M, Zhang C, Michaels R, Restrepo D, Ottersen OP, Olson C, Nagy JI. Ultrastructural localization of connexins (Cx36, Cx43, Cx45), glutamate receptors and aquaporin-4 in rodent olfactory mucosa, olfactory nerve and olfactory bulb. J Neurocytol. 2005; 34:307–341. [PubMed: 16841170]

Rash JE, Dillman RK, Bilhartz BL, Duffy HS, Whalen LR, Yasumura T. Mixed synapses discovered and mapped throughout mammalian spinal cord. Proc Natl Acad Sci (USA). 1996; 93:4235–4239. [PubMed: 8633047]

Rash, JE.; Johnson, TJA.; Dinchuk, JE.; Giddings, FD.; Kuenning, W. Labeling intramembrane particles and surface markers in freeze-etch replicas. In: John, JB.; Berlin, E.; Jackson, PC., editors. Frontiers of Membrane Research in Agriculture. Totowa,NJ: Rowman & Allenheld; 1983. p. 7-22.

Rash JE, Pereda A, Kamasawa N, Furman CS, Yasumura T, Davidson KGV, Dudek FE, Olson C, Nagy JI. High-resolution proteomic mapping in the vertebrate central nervous system: Close proximity of connexin35 to NMDA glutamate receptor clusters and co-localization of connexin36 with immunoreactivity for zonula occludens protein-1 (ZO-1). J Neurocytol. 2004; 33:131–152. [PubMed: 15173637]

Rash JE, Pickard GE, Davidson KGV, O'Brien J, Hartwick ATE, Kamasawa N, Yasumura T, Nagy JI. Exposure to dopamine and its D1 receptor antagonist SCH23390 produces large-scale ultrastructural plasticity and changes in phosphorylation of connexin36 in neuronal gap junctions of adult rat retina. Mol Biol Cell. 2007; 18(supplement) Abstract #910.

Rash JE, Yasumura T. Direct immunogold labeling of connexins and aquaporin4 in freeze-fracture replicas of liver, brain and spinal cord: factors limiting quantitative analysis. Cell Tissue Res. 1999; 296:307–321. [PubMed: 10382274]

Rash JE, Yasumura T, Dudek FE, Nagy JI. Cell-specific expression of connexins, and evidence for restricted gap junctional coupling between glial cells and between neurons. J Neurosci. 2001; 21:1983–2001. [PubMed: 11245683]

Robertson JD, Bodenheimer TS, Stage DE. The ultrastructure of Mauthner cell synapses and nodes in goldfish brains. J Cell Biol. 1963; 19:159–199. [PubMed: 14069792]

Sato Y, Nishida M. Teleost fish with specific genome duplication as unique models of vertebrate evolution. Environ Biol Fish. 2010; 88:169–188.

Schlörmann W, John M, Steiniger F, Westermann M, Richter W. Improved antigen retrieval in freeze-fracture cytochemistry by evaporation of carbon as first replication layer. Histochem Cell Biol. 2007; 127:633–639. [PubMed: 17415584]

Serrano-Vélez JL, Rodriguez-Alvarado M, Torres-Vázquez II, Fraser SE, Yasumura T, Vanderpool KG, Rash JE, Rosa-Molinar E. Abundance of gap junctions at glutamatergic mixed synapses in adult Mosquitofish spinal cord neurons. Front Neural Circuits. 2014; 8 Article 66:1–16. [PubMed: 24478635]

Sotelo C, Korn H. Morphological correlates of electrical and other interactions through low-resistance pathways between neurons of the vertebrate central nervous system. Internat Rev Cytol. 1978; 55:67–107.

Steere RL, Erbe EF. Supporting freeze-etch specimens with ‘Lexan’ while dissolving biological remains in acids. Microsc Soc Am Proc. 1983; 41:618–619. Published Abstract.

Steere, RL.; Rash, JE. Use of double-tilt device (goniometer) to obtain optimum contrast in freeze-fracture replicas. In: Rash, JE.; Hudson, CS., editors. Freeze fracture: Methods, Artifacts, and Interpretations. New York: Raven Press; 1979. p. 161-167.

Trenholm S, McLaughlin AJ, Schwab DJ, Awatramani GB. Dynamic tuning of electrical and chemical synaptic transmission in a network of motion coding retinal neurons. J Neurosci. 2013; 33:14927–14938. [PubMed: 24027292]

Tuttle R, Masuko S, Nakajima Y. Freeze-fracture study of the large myelinated club ending synapse on the goldfish Mauthner cell: Specialized reference to the quantitative analysis of gap junctions. J Comp Neurol. 1986; 246:202–211. [PubMed: 3007585]

Uchiyama H, Ito H. Fiber connections and synaptic organization of the preoptic retinopetal nucleus in the filefish (Balistidae, Teleostei). Brain Res. 1984; 298:11–24. [PubMed: 6722548]

Witkovsky P, SHAKIB M, Ripps H. Interreceptoral junctions in the teleost retina. Invest Opthal Vis Sci. 1974; 13:996–1009.

Wolburg H, Rohlmann A. Structure-function relationships in gap junctions. Internat Rev Cytol. 1995; 157:315–373.

Yao C, Vanderpool KG, Delfiner M, Eddy V, Lucaci A, Soto-Riveros C, Yasumura T, Rash J, Pereda AE. Electrical synaptic transmission in developing zebrafish: properties and molecular composition of gap junctions at a central auditory synapse. J Neurophysiol. 2014; 112:2102–2113.10.1152/jn.00397.2014 [PubMed: 25080573]

Zupanc GKH. Clustering of cell bodies, bundling of dendrites, and gap junctions: morphological substrate for electrical coupling in the prepacemaker nucleus. Neurosci Let. 1991; 129:29–34. [PubMed: 1922968]

Abbreviations

CE	club ending (size of terminal and state of myelination not determinable)
CNS	central nervous system
CT	carboxy terminus
Cx34.7	connexin34.7
Cx35	connexin35
Cx36	connexin36
Cx45	connexin45
Cx57	connexin57
DR-FRIL	double-replica FRIL
DR-SDS-FRL	double-replica SDS-freeze-fracture labeling
FRIL	freeze-fracture replica immunogold labelling
FRL	fracture replica labeling (*i.e.*, FRIL without confocal microscopic mapping)
LMCE	large myelinated club ending
IgG	immunoglobulin
IL	intracellular loop
IMP	intramembrane particle
LBB	labeling blocking buffer
M-Cell	Mauthner cell
NMDA	n-methyl-D-aspartate
NMDAR1	NMDA glutamate receptor subunit 1
PBS	sodium phosphate buffered 0.9% saline
RSN	reticulospinal neuron
SDS	sodium dodecyl sulfate
SV	synaptic vesicle
TBS	Tris buffered saline
TBSTr	TBS containing Triton X-100

Highlights

Immunocytochemical labeling reveals that neuronal gap junctions are abundant and widely distributed in goldfish brain.

Cx35/Cx34.7-containing gap junctions occur primarily at glutamatergic axon terminals, forming excitatory “mixed” synapses.

Immunogold labeling for Cx35 was only in axon terminal hemiplaques and for Cx34.7 only in somatic and dendritic hemiplaques.

Widespread Cx35**:**Cx34.7 heterotypic coupling may imply widespread electrical rectification.

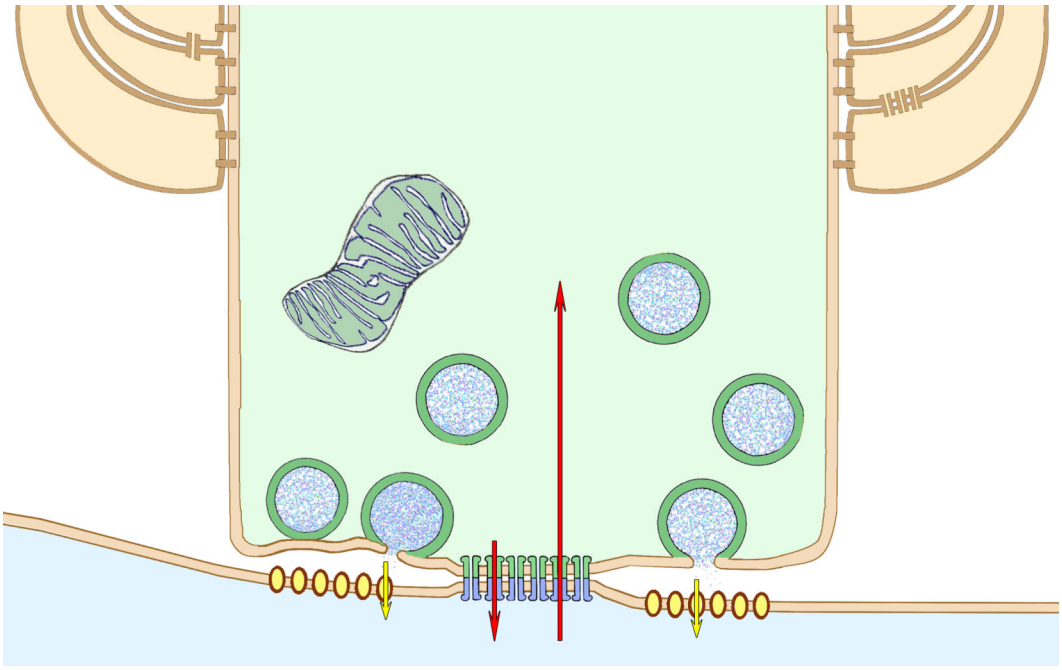

Fig. 1.

Schematic diagram of large myelinated club ending (LMCE) forming a glutamatergic mixed synapse onto a Mauthner cell dendrite. “Large” (50-nm) round, clear synaptic vesicles (with blue stippling for glutamate) are characteristic of excitatory chemical synapses. Long *vs.* short red arrows indicate bi-directional but asymmetric 4:1 electrical conductance (*i.e.*, electrical rectification), with the preferred direction of current flow (longer arrow) from the postsynaptic to the presynaptic compartment. In the gap junction, the connexins have 100% asymmetric distribution in apposing hemiplaques, with Cx35 present only in axon terminal hemiplaques (green connexons) and Cx34.7 only in somatic and dendritic hemiplaques (blue connexons), as previously described (Rash et al., 2013). Yellow arrows indicate unidirectional chemical synaptic transmission. Myelin = beige overlay; LMCE = green overlay, dendrite = blue overlay, yellow ovals = glutamate receptors.

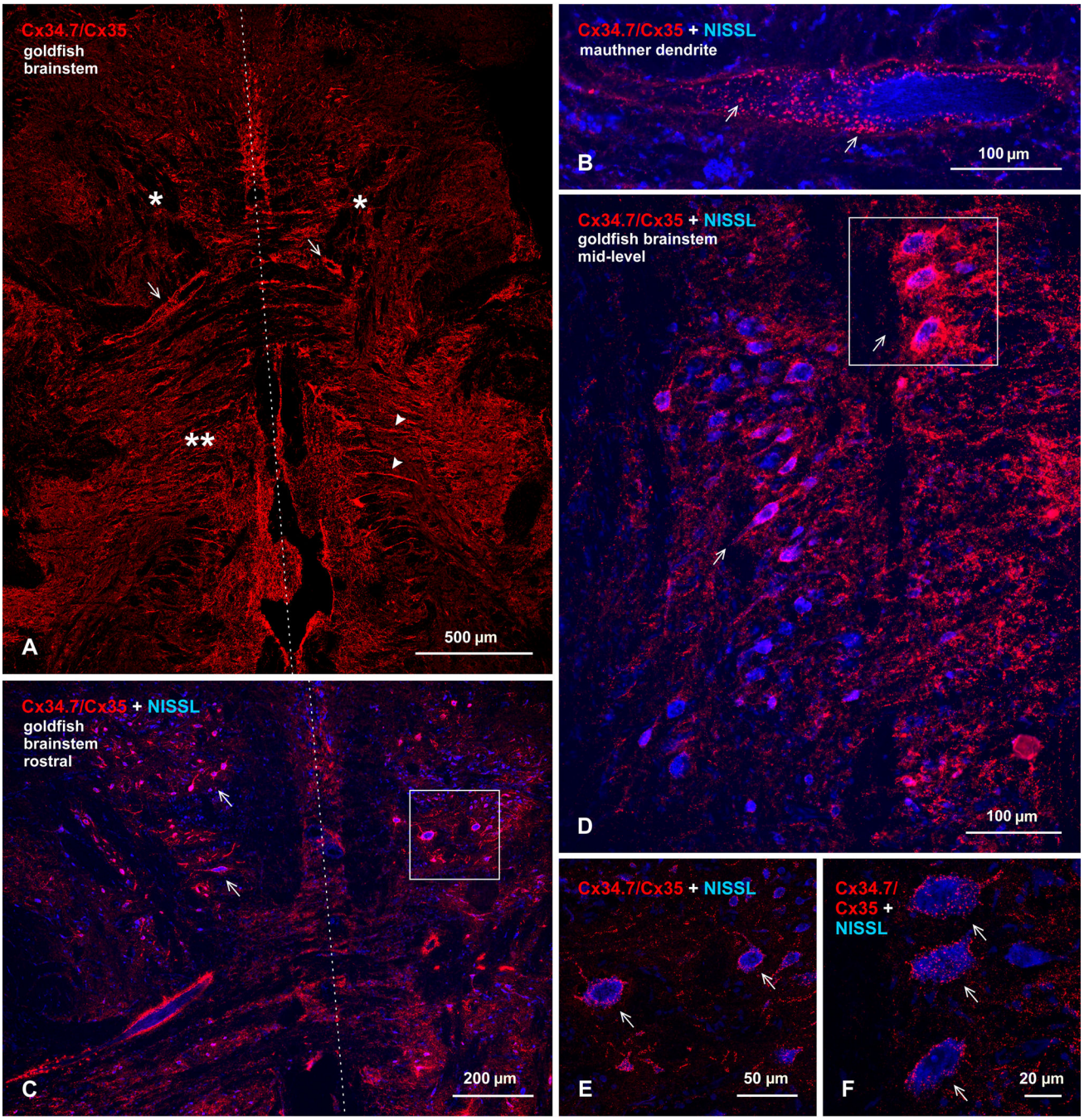

Fig. 2.

Immunofluorescence image showing abundance of Cx34.7/Cx35 puncta in horizontal sections at a rostral level of goldfish hindbrain and at a dorsal-ventral level of the Mauthner cell (M-cell). Some of the images are shown with blue fluorescence Nissl counterstaining. (A) Low magnification bilateral overview (dotted line indicates midline), showing a high density of immunofluorescent puncta associated with M-cell lateral dendrites (arrows), and similarly dense puncta at more rostral (single asterisk) and caudal (double asterisk) regions to the M-cell, including labeling along bundles of laterally directed dendrites (arrowheads).

(B) Magnification of M-cell dendrite, showing numerous patches of labeling (arrows) localized to the dendritic surface. (C,D) Rostral and caudal regions indicated by single and double asterisks in A are shown in C and D, respectively, but taken from different sections and magnified. At the rostral level, groups of large neurons on either side of the midline are outlined by labeling of Cx34.7/Cx35 puncta on their somata and dendrites (C, arrows). At the more caudal level shown unilaterally, large neurons located medially (D, upper arrow, in boxed area) and medium size neurons located laterally (D, lower arrow) are heavily laden with punctate labeling (widefield multiple scan Z-stack). (E,F): Higher-magnification confocal scans of boxed areas in C and D, respectively, showing exclusively punctate appearance of labeling associated with neuronal somata (arrows). Image in F (from box in D) is magnified still further in Figure 8A. Calibration bars are labeled individually on each image.

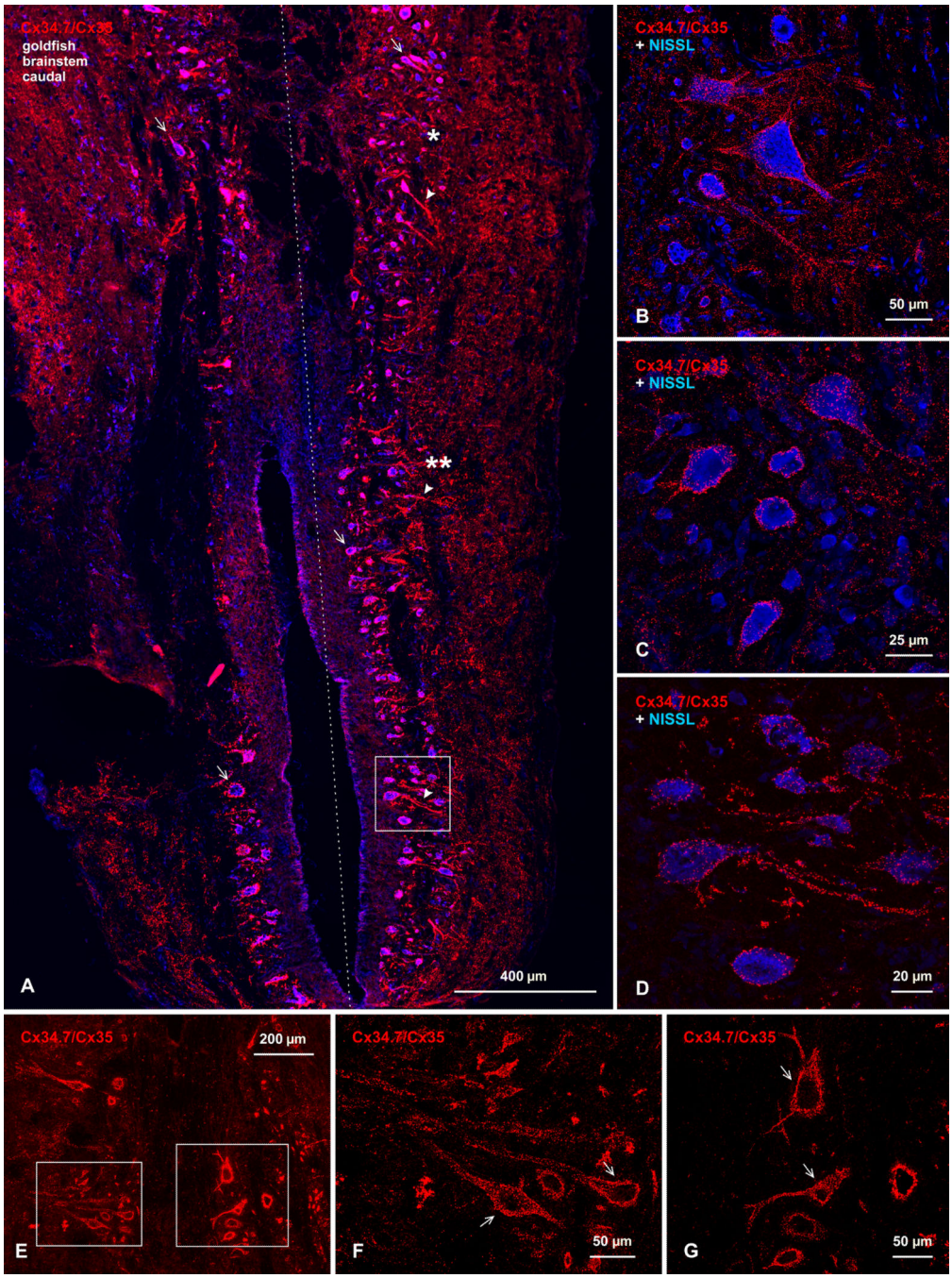

Fig. 3.

Immunofluorescence image of Cx34.7/Cx35 puncta in horizontal sections of the caudal portion of goldfish hindbrain at a rostro-caudal level of brainstem-spinal cord transition. Shown with and without blue fluorescence Nissl counterstaining. (A) Low magnification bilateral overview (dotted line indicates midline), showing collections of neurons on each side of the midline decorated with labeling for Cx34.7/Cx35 puncta around their somata (arrows) and along their laterally directed dendrites (arrowheads). A moderate density of labeling is seen distributed in more lateral regions of neuropil. (B-D) Regions indicated by

single and double asterisks in A are shown in B and C, respectively, but taken by confocal scanning from different sections, and the boxed area in A is shown at higher magnification in D. In all regions, images show punctate appearance of immunolabeling, with no evidence of intracellular labeling. (E-G) Images of brainstem neurons taken for counts of Cx34.7/Cx35-puncta associated with neuronal somata (F,G arrows) and their initial dendrites. Images in F and G are magnifications of the boxed areas in E. Calibration bars are labeled individually on each image.

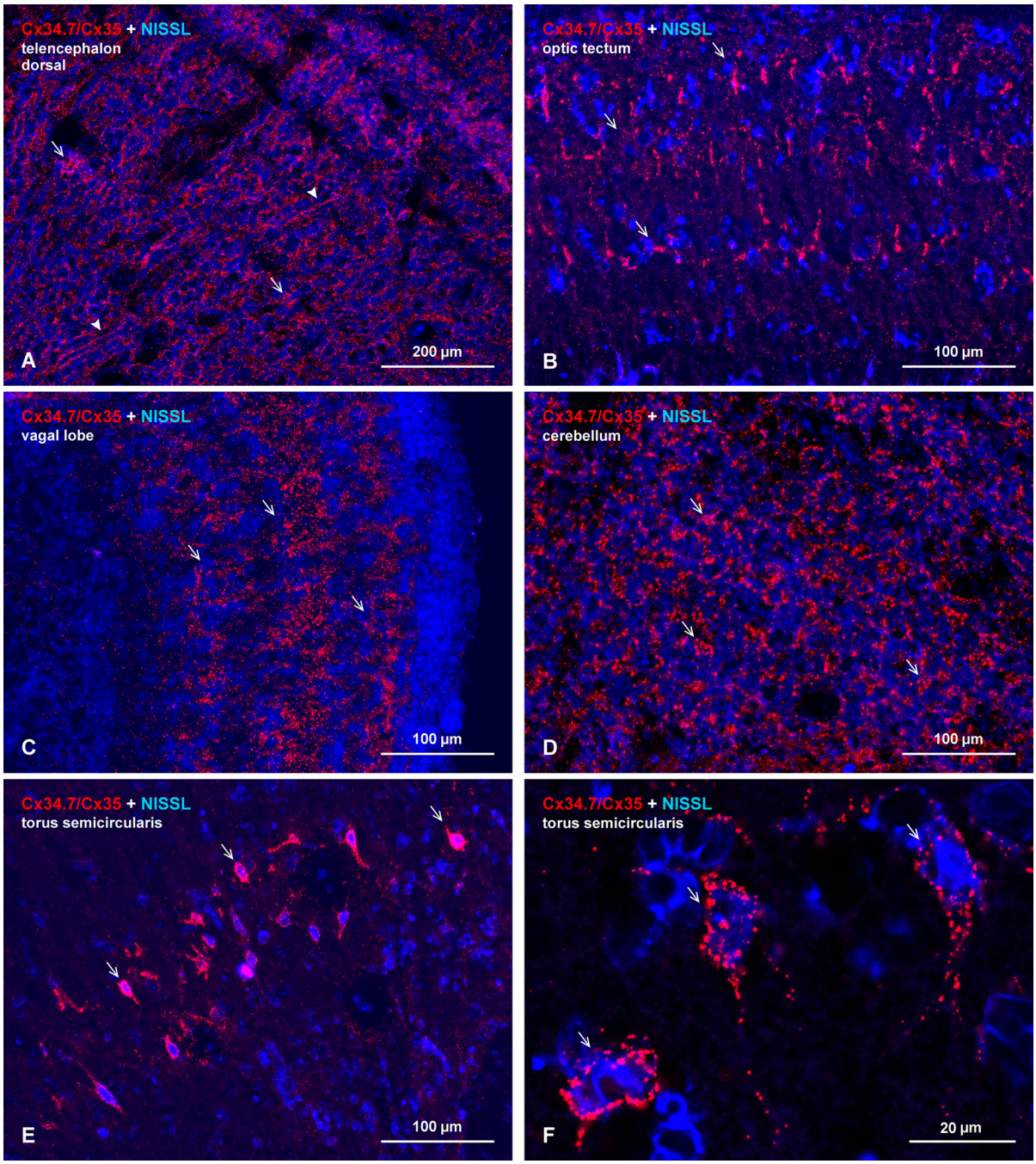

Fig. 4.

Immunofluorescence image revealing abundant Cx34.7/Cx35 puncta in selected regions of goldfish forebrain, shown in horizontal sections with blue fluorescence Nissl counterstaining. (A) Dorsal telencephalon, with dense immunolabeling scattered throughout and with greater abundance localized to patches of neuropil (arrows) or along dendrites directed towards the cortical surface (arrowheads). (B,C) Optic tectum and vagal lobe, both organized as laminar structures, with moderate immunolabeling localized to superficial, middle and deep lamina in the tectum (B, arrows) and dense dispersed labeling distributed

also in three lamina of the vagal lobe (C, arrows). (D) Cerebellum, showing a high density of immunofluorescent puncta in the granule cell layer, with labeling clustered in relatively uniform size patches (arrows). (E,F) Torus semicircularis; labeling is sparse in most regions, except for puncta heavily concentrated on the somata and initial dendrites of a group of neurons arranged in an arc (E, arrows) spanning the length of this structure. As elsewhere, only higher magnification reveals the punctate nature of this labeling (F, arrows). Calibration bars are labeled individually on each image.

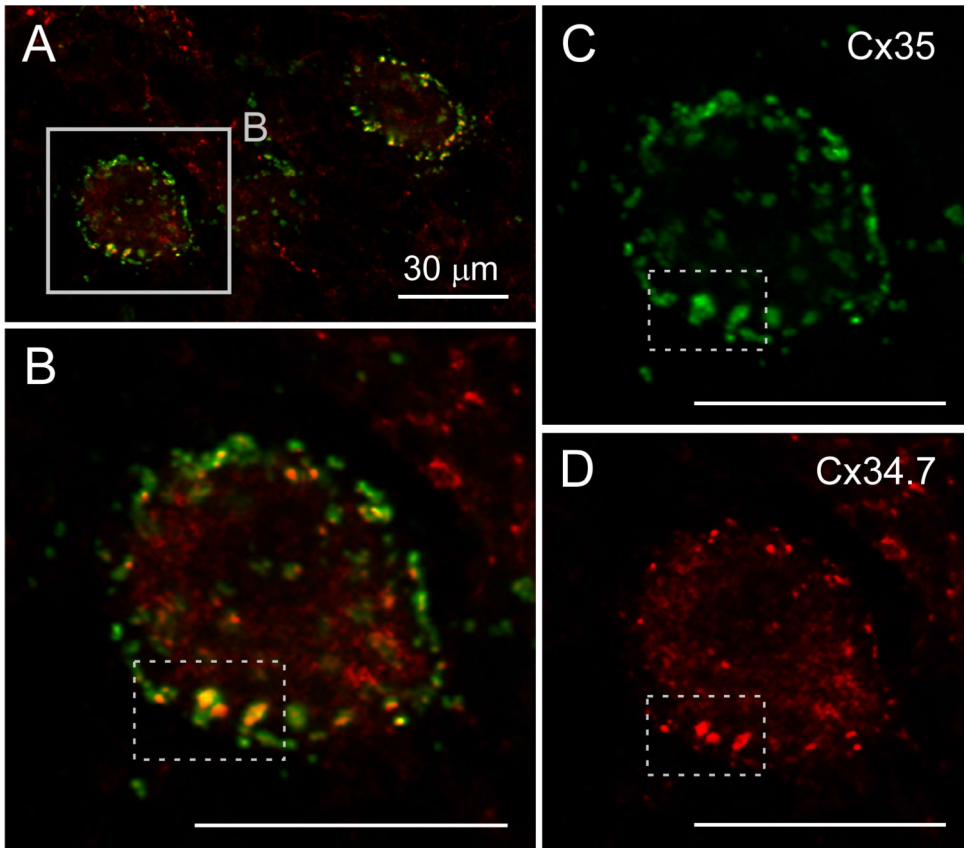

Fig. 5.

Co-localization of Cx35 and Cx34.7 at individual synapses on neurons of the goldfish hindbrain. Double immunolabeling with a monoclonal Cx35 antibody (green) and the polyclonal Cx34.7 IL antibody (red) shows a high degree of co-localization on RSNs in the goldfish hindbrain. (B) Higher magnification of one of the RSNs showing high co-localization of intense punctate labeling for Cx35 (C) and Cx34.7 (D), evident in the selected areas (dotted boxes). Calibration bars are 30 μm.

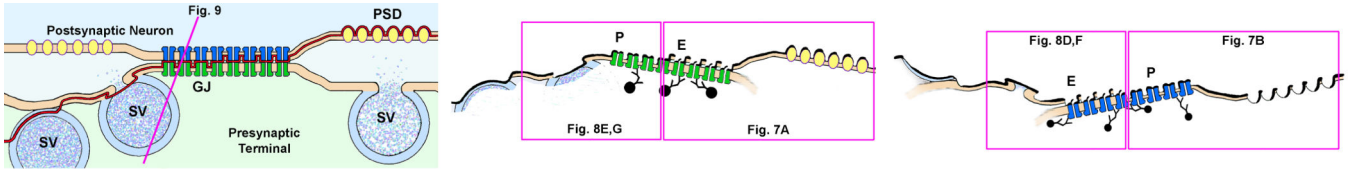

Fig. 6.

Drawings of DR-FRIL matched double-replicas of a gap junction between axon terminal and neuronal dendrite (A), simultaneously double-labeled for Cx35 (B) and Cx34.7 (C). Labeling pattern reveals solely pre-synaptic Cx35 (B; 10-nm gold beads) and post-synaptic Cx34.7 (C; 5-nm gold beads), illustrating heterotypic coupling of presynaptic Cx35 to postsynaptic Cx34.7. Connexin labeling occurs only on cytoplasmic epitopes remaining beneath the replica, regardless of whether the P-face particles of the lower cell (B; left panel, and C, left side of right panel) or the E-face pits of the upper cell (B; right panel and C, left panel) are visualized in the replica. Blue line in A and small figure numbers in B and C refer to corresponding text figures. Glutamate receptors (A,B, yellow ovals) remain with the E-face as “intramembrane particles” and leave corresponding “pits” in the complementary P-face (C, small depressions in right panel).

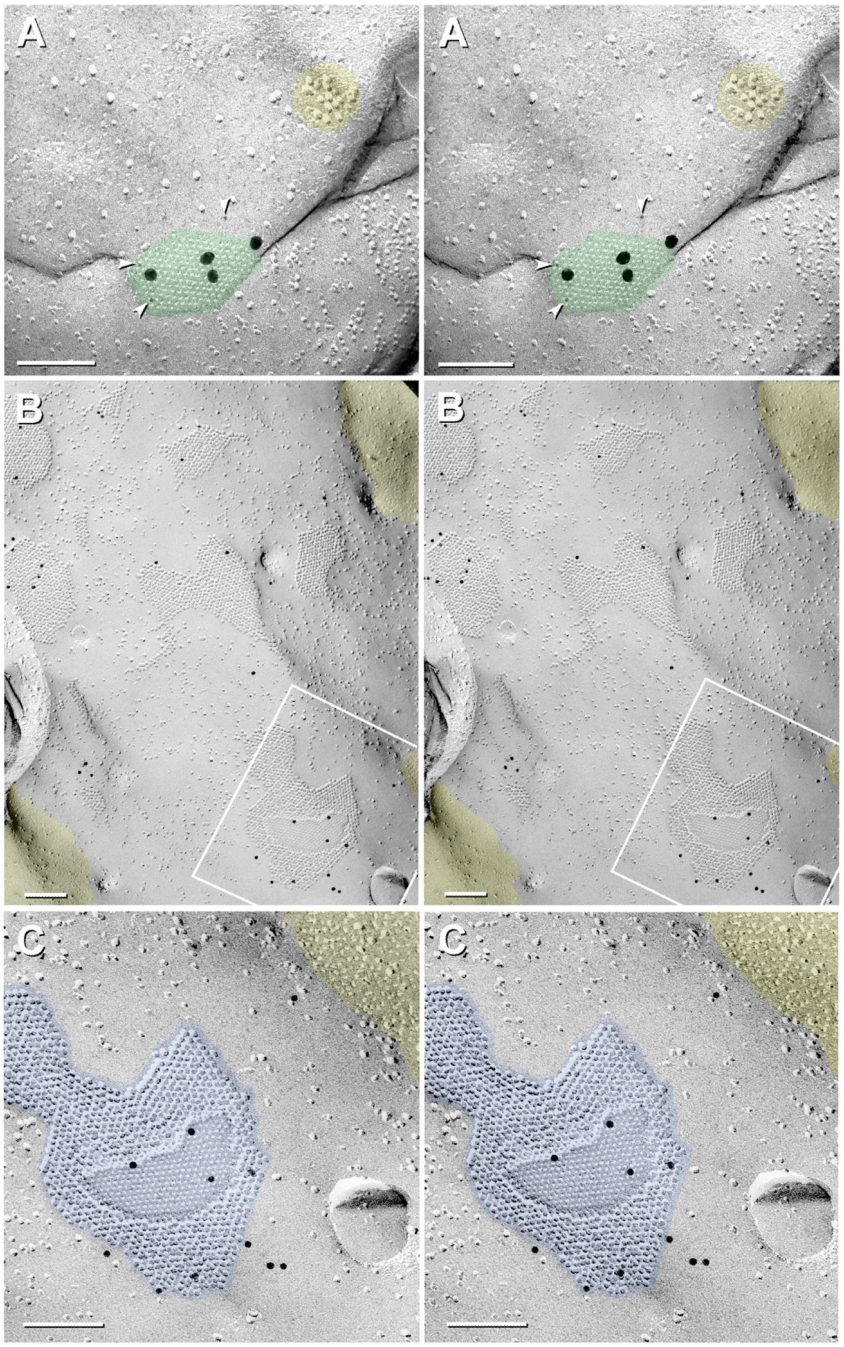

Fig. 7.

FRIL image of simultaneous Cx35 presynaptic and Cx34.7 postsynaptic labeling in the same replica (R811). (A) Cx35 labeling (three 6-nm, arrowheads, two 18-nm, and two 20-nm gold) in a small gap junction hemiplaque viewed toward the CE on an RSN found *ca*. 450 μm form the M-cell. (B,C) Low and high magnification stereoscopic views of 11 M-cell gap junctions labeled for Cx34.7. A few 10-nm (rabbit) and 12-nm (chicken) gold beads label nine of the 11 gap junctions shown in B (from total of 81 gap junctions exposed in this LMCE/M-cell contact). (C) Higher magnification view of one large gap junction that is

labeled by 10 10-nm and 12-nm gold beads, which are difficult to separately distinguish. Yellow overlays indicate glutamate receptor E-face particles in the RSN plasma membrane (A) and P-face pits representing where glutamate receptor proteins had been removed from the M-cell P-face (B,C). The 100% differential labeling in A *vs.* B and C (*i.e.,* labeling for one connexin but no labeling for the other connexin) is consistent with heterotypic Cx35:Cx34.7 coupling. Note: Images A and C are at the same magnification, revealing that the gold beads for Cx35 vs. Cx34.7 are distinctly different in size. Calibration bars are 0.1 μm.

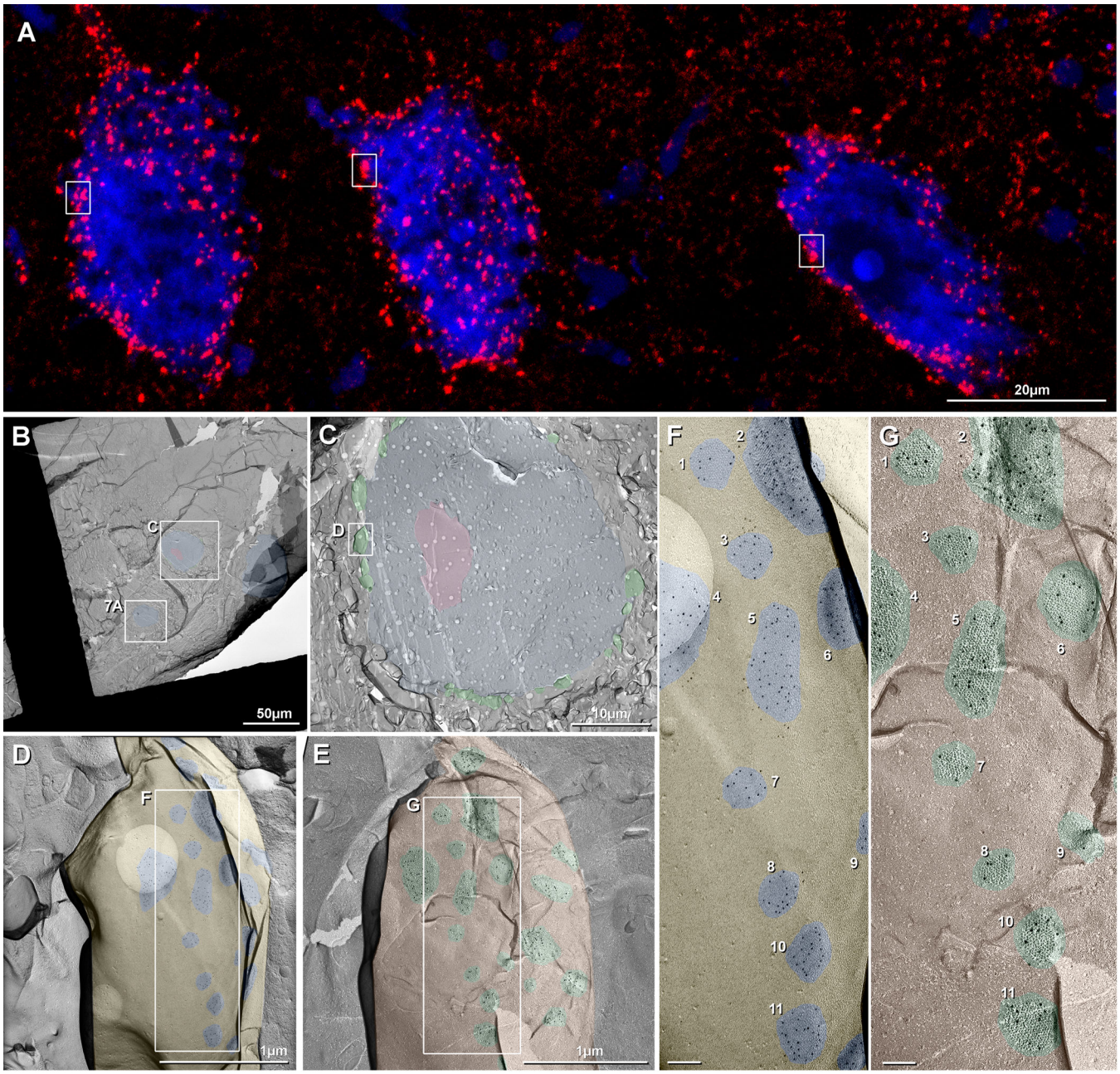

Fig. 8.

Immunofluorescence (A) and FRIL images (B-G) of goldfish reticulospinal neurons (RSN). (A) Higher magnification image from Fig. 1F, showing >1000 immunofluorescent puncta on the somata and proximal dendrites of three neurons. For comparative purposes, boxes delineating individual large club endings are the same anatomical size in A and C. (B) FRIL overview image of a cluster of three neurons (*blue overlays*) in rhombomere R5. All RSN neurons had multiple small and large club endings along their perimeters. (C) Magnified image of Box C in B, presented at the same magnification as A. Pink overlay = cross fractured nucleus. (D,E) Higher magnification image of Box D in C, containing a single large CE, and shown as a complementary matched double replicas of the E-face (D) and P-

face (E) of a portion of that large club ending, from matched “DRD top” and “DRD bottom”. Nineteen of the *ca.* 24 gap junctions are seen in the E-face image (D, blue overlays), and the same 19 gap junctions are seen in the complementary P-face image (E; green overlays). (F,G) Higher magnifications of the boxed areas in D,E, showing matched double replicas of 11 of the same gap junctions (numbered 1-11), 100% of which are labeled for Cx34.7 (5-nm gold beads) in E-face images of the club endings, as viewed toward the underlying RSN (F). Conversely, 100% of presynaptic hemiplaques are labeled exclusively for Cx35 (10-nm gold beads beneath axon terminal P-face particles) (G). Calibration bars are as indicated in A-E and are 0.1 μm in F,G.

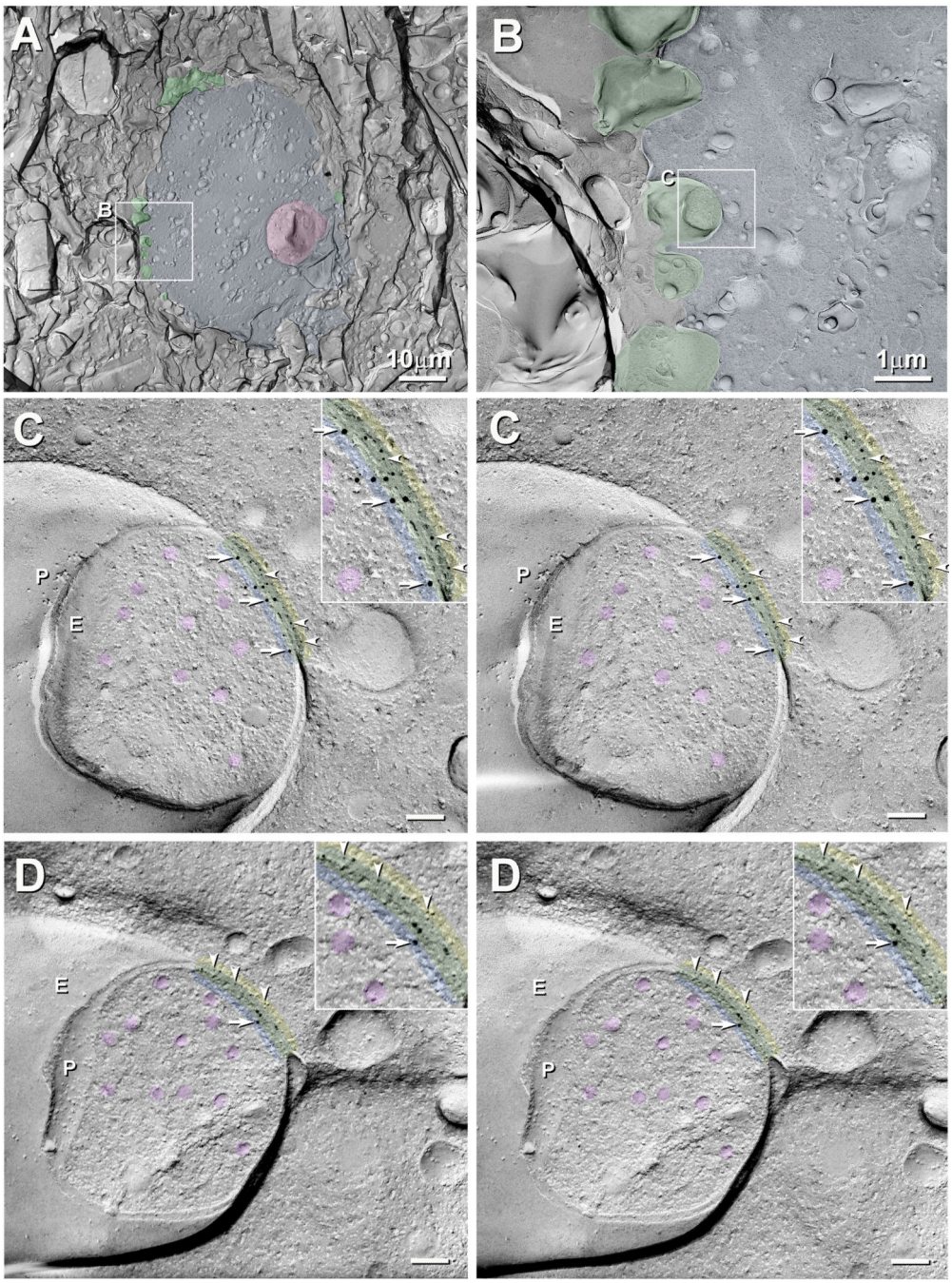

Fig. 9.

Low to high-magnification images of cross-fractured mixed synapse in matched double-replicas from RSN (from the red line labeled “9A” in Fig. 6B. (A) Low magnification image of RSN (blue overlay) and surrounding neuropil. RSN nucleus is to the right (pink overlay); axon terminals (several delineated by green overlays) surround the entire neuronal soma. (B) Magnified image of the boxed area in A, showing a portion of RSN cytoplasm (blue overlay) and five of >30 axon terminals (green overlays). (C,D) Higher magnification stereoscopic image of boxed area in B, shown as matched complementary replicas, wherein

P-faces in (C) are matched by E-faces in (D), and vice versa. A cross-fractured gap junction is double-labeled in both images, with Cx35 (10-nm gold beads) in the axon terminal cytoplasm in both images (blue strip overlays), and Cx34.7 (5-nm gold beads; arrowheads) in the postsynaptic cytoplasm in both stereoscopic images (yellow strip overlays). Because of the 28-nm radius of immunogold labeling [“radius of uncertainty”(Fujimoto, 1995; Fujimoto, 1997; Kamasawa et al., 2006)], the area of potential overlap of immunogold labeling is indicated by intervening green strip overlays. Lavender overlays indicate matching structural details in the two images, including several round/hemispherical synaptic vesicles, which combined with the gap junction, positively identify this as an excitatory (probably glutamatergic) mixed synapse. Calibration bars are 0.1 μm.

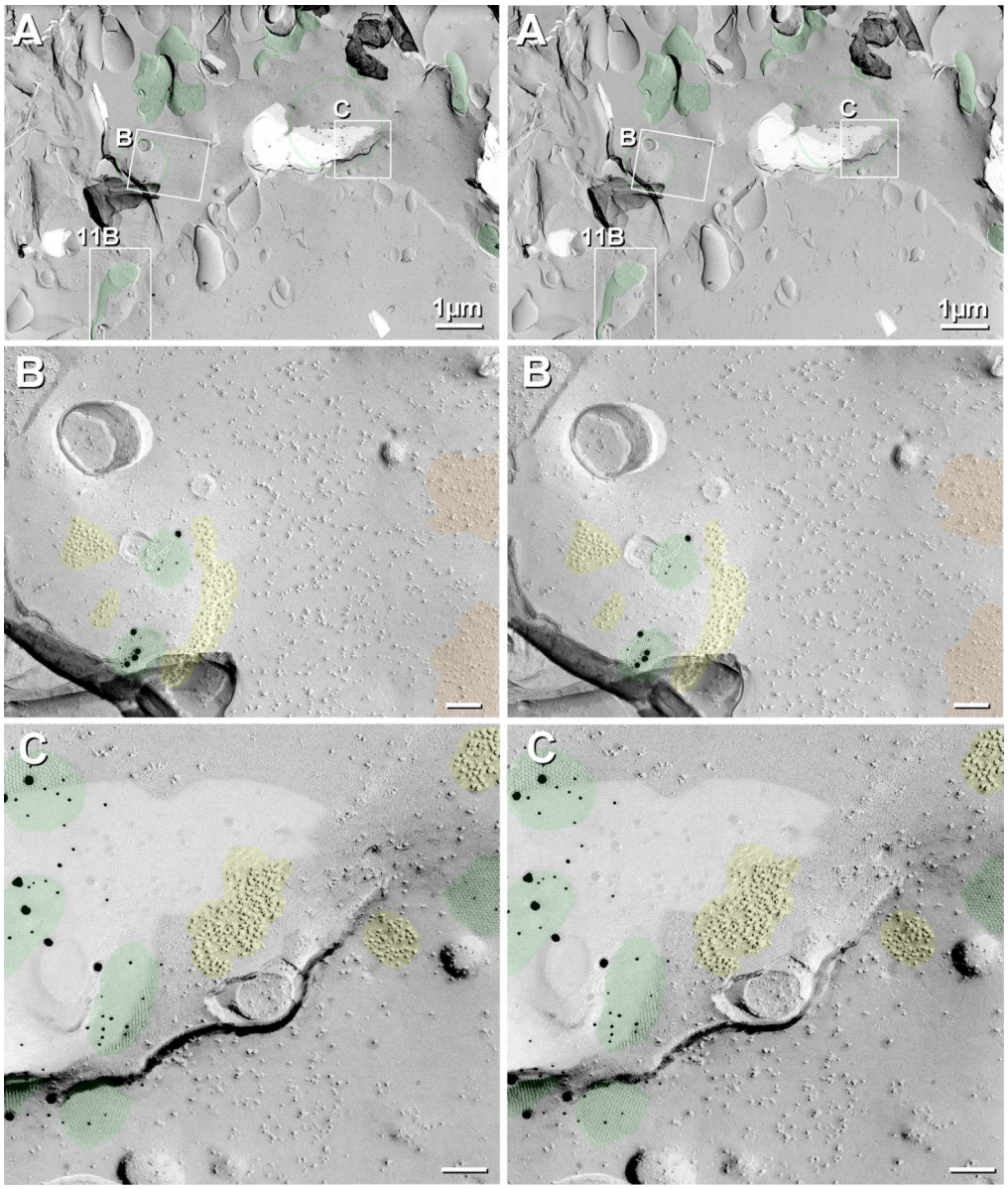

Fig. 10.

Band of closely-spaced glutamatergic mixed synapses on RSN. (A) Low magnification overview of glutamatergic mixed synapses on soma of RSN. Boxes are enlarged in subsequent images. (B) Higher magnification image of Box B in A, revealing a gap junction that is immunogold labeled for Cx35 by 5-nm and 20-nm gold beads (green overlay), closely surrounded by clusters of 10-nm E-face IMPs that are identified as glutamate receptors. At the right edge are equally distinctive clusters of E-face pits (orange overlays) identified as PSDs of inhibitory synapses, presumably representing the impressions of GABA receptors or glycine receptors, which were never closer than 0.3-0.5 µm to gap junctions. At a larger scale, inhibitory synapses are often intermingled with excitatory synapses on the lateral dendrite (Nakajima et al., 1987), but are spatially segregated near the axon hillock (see Fig. 12). (C) Portion of an LMCE synapse (enlarged from Box C in Fig. 10A) onto the RSN E-

face. Immunogold-labeled gap junctions (green overlays) are interspersed with E-face particle clusters that we have identified as NMDA R1-containing glutamate receptor PSDs. Calibration bars = 1 μm (A) and 0.1 μm (B,C)

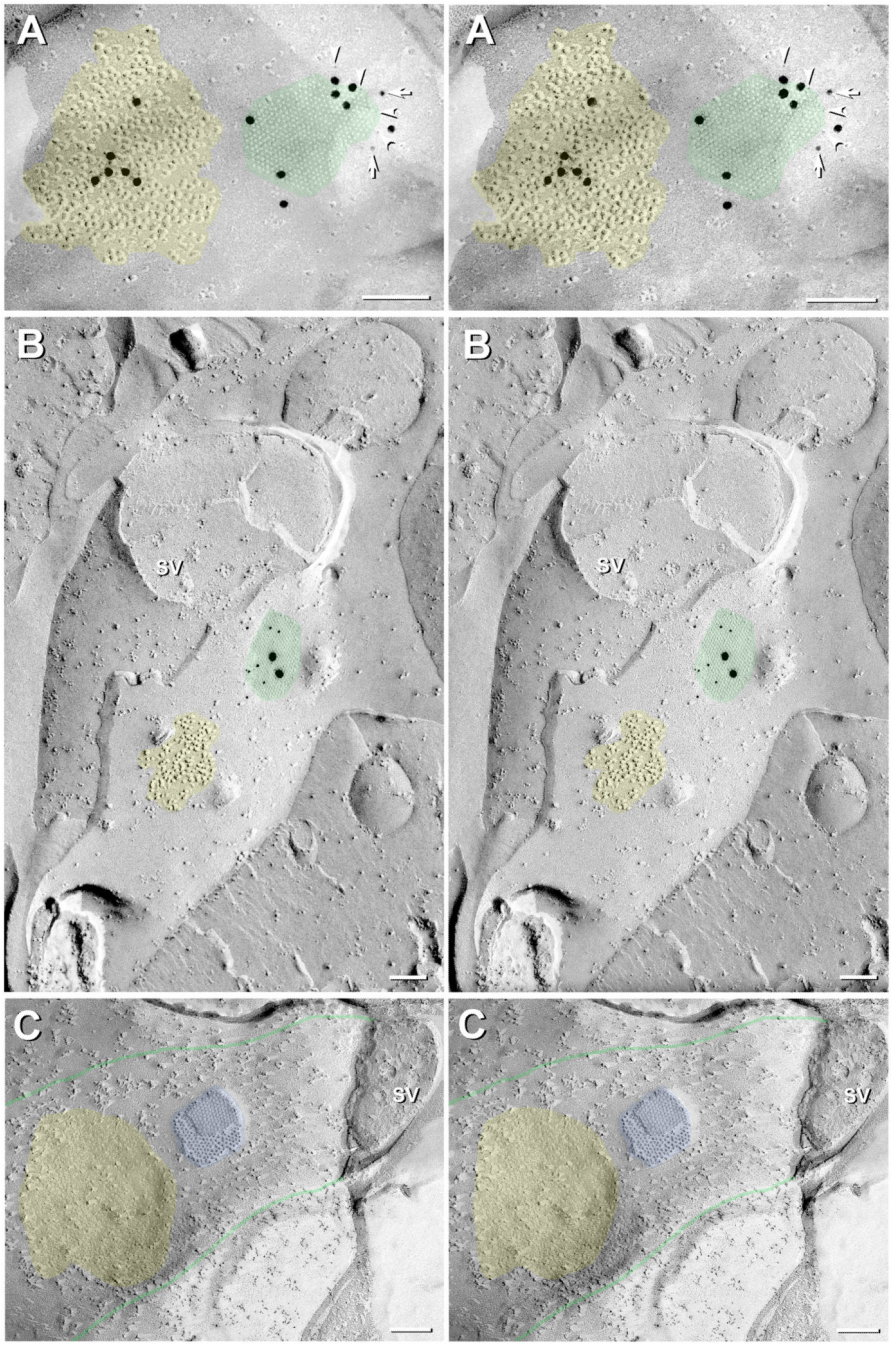

Fig. 11.

Stereoscopic FRIL images from goldfish hindbrain, illustrating several criteria used to identify glutamatergic mixed synapses. (A,B) Synapses on neuronal somata and dendrites are positively identified as glutamatergic mixed synapses based on presence of gap junctions plus glutamate receptor E-face particles (Pereda et al., 2003; Rash et al., 2004; Rash et al., 2005; Kasugai et al., 2010; Hamzei-Sichani et al., 2012; Nagy et al., 2013; Serrano-Vélez et al., 2014), which in were immunogold labeled by 18-nm gold beads, only (A) (see Sequential Labeling in Experimental Procedures). However, the gap junction inking to the

subjacent axon terminal was triple labeled, first for Cx35 by 6-nm (arrowheads) and 12-nm (arrows), followed by 18-nm gold beads. This and similar glutamate receptor PSDs were almost always immediately adjacent to (0.03 to 0.15 μm away from) the immunogold-labeled gap junction. See Fig. 6H-J for diagrammatic explanation of connexin labeling in the residual cytoplasm of the axon terminal beneath E-face pits *vs.* NMDA R1 labeling of E-face particles in the subjacent extracellular space. (B) FRIL image of an axon terminal embedded into the E-face of an RSN soma (enlarged from Box 11B in Fig. 10A). The distinctive E-face particle cluster (yellow overlay) represents a PSD that is ca. 0.3 μm away from the cross-fractured axon terminal cytoplasm, the distance accounting for the relatively few 50-nm round synaptic vesicles (SV) that characterize excitatory synapses (Landis et al., 1974; Landis and Reese, 1974; Harris and Landis, 1986). Both 5-nm and 20-nm gold beads label Cx35, whereas glutamate receptors were not labeled in this replica. (C) P-face view of dendrite in goldfish hindbrain, with unlabeled gap junction (blue overlay) immediately adjacent to area where glutamate receptors had been removed, leaving closely clustered pits (yellow overlay). For unknown technical reasons, labeling for Cx34.7 was unsuccessful in this and all replicas made that same day. Most of the axon terminal was removed, leaving an elongate depression (margins delineated by green lines) that contains the gap junction (blue overlay) and the P-face pits that resulted from removal of the densely-clustered glutamate receptors (yellow overlay). SV = synaptic vesicles. Calibration bars are 0.1 μm.

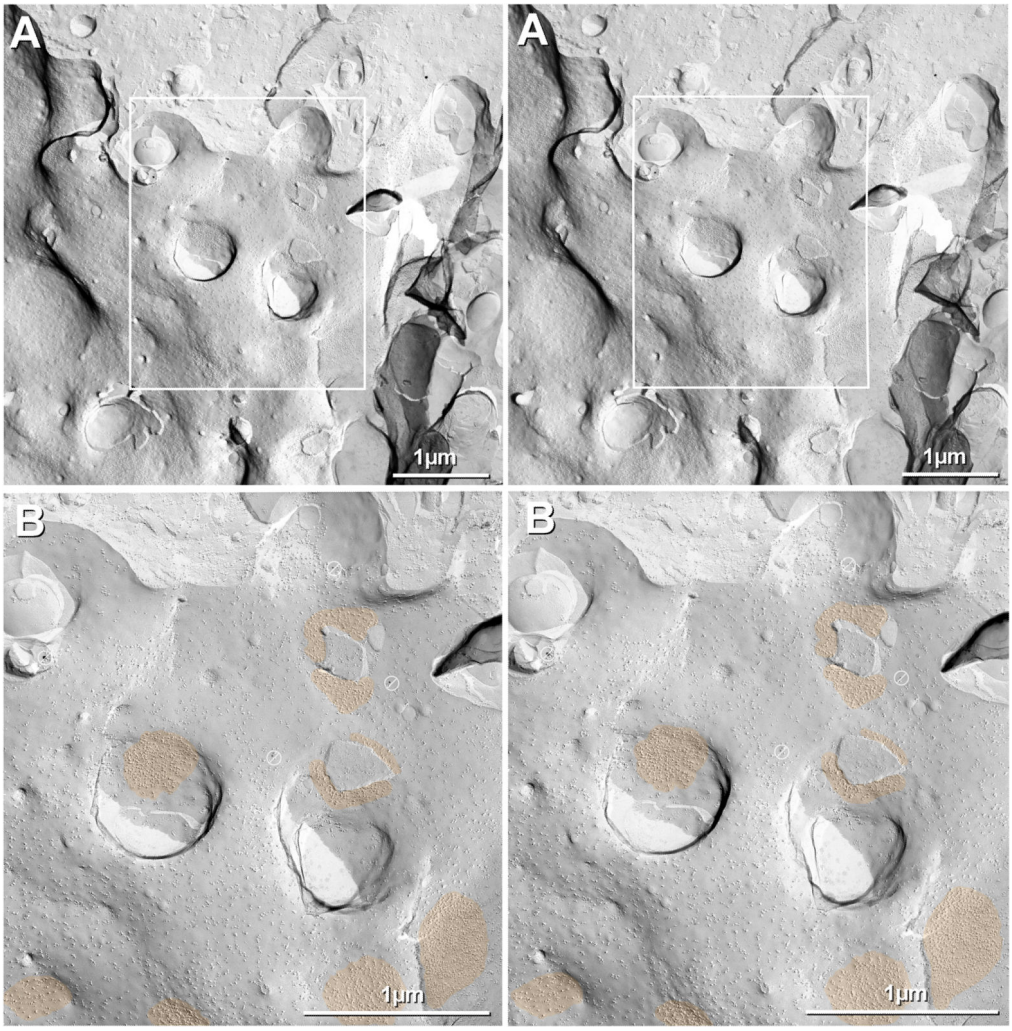

Fig. 12.

Low and high magnification stereoscopic images of *ca.* 20 inhibitory synapses (GABAergic and probable glycinergic) tightly localized on an unidentified neuron in goldfish vagal lobe (dorsal surface of hindbrain). Most excitatory and inhibitory chemical synapses create 0.5 µm- to 1 µm-diameter cuplike indentations of the somatic and dendritic plasma membrane (A; enlarged in B), but some form flattened appositions (B) having P-face particle clusters that represent primarily GABA receptors (Kasugai et al., 2010) and possibly glycine receptors. Two active zones (not colored) overlie P-face PSDs (yellow overlays at upper right). Barred circles designate gold beads on the top of the replica, thereby representing positively-identified background “noise”, which is minimal in all images shown. Calibration bars = 0.1 µm.

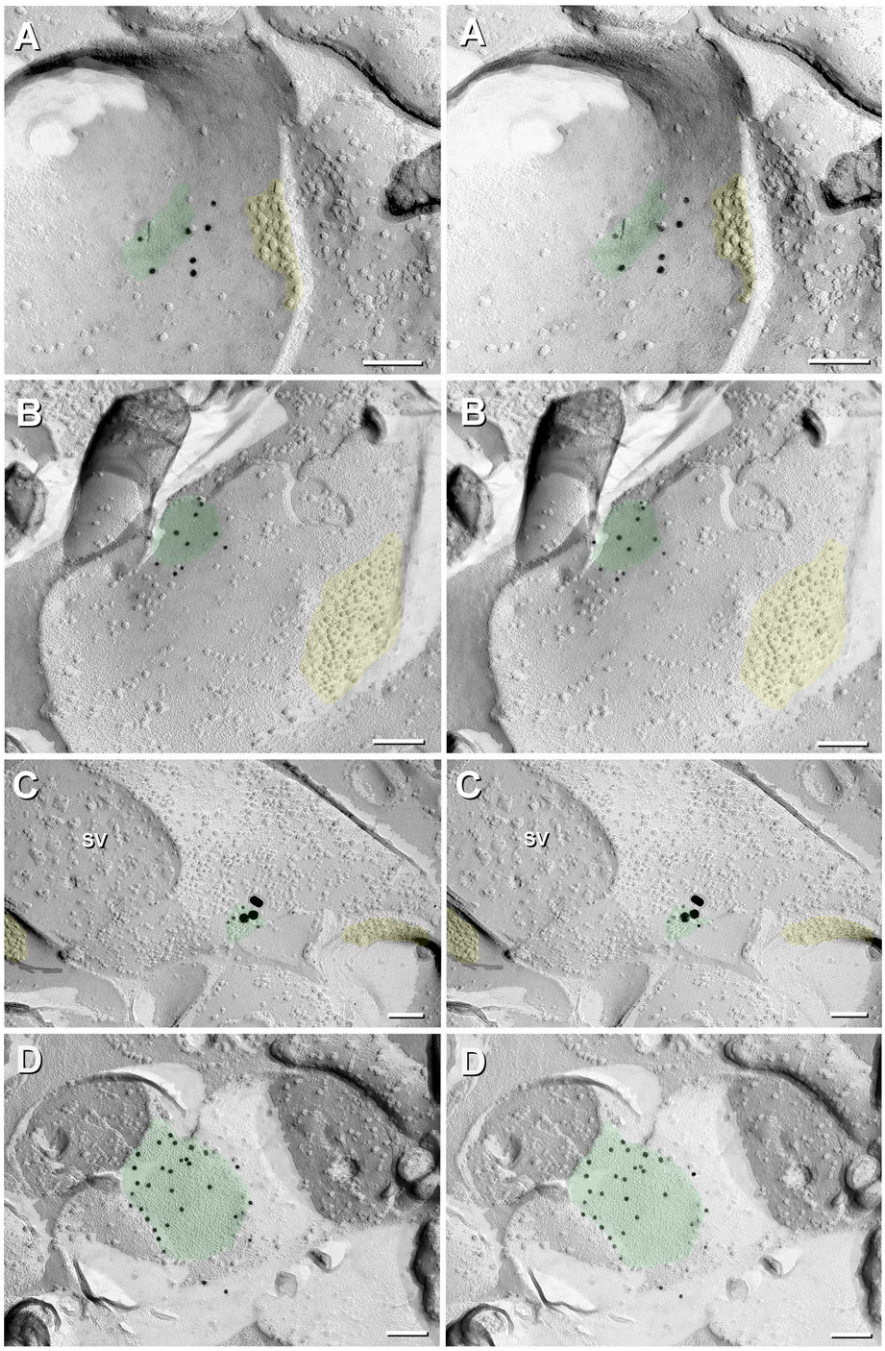

Fig. 13.

Gap junctions at probable glutamatergic mixed synapses in corpus cerebelli (aka cerebellum) (A,B) and optic tectum (C), and unidentified electrical synapse in corpus cerebelli between a small dendrite (D, right side, containing 80-nm Golgi vesicles) and an unidentified neurite (D, top left), possibly corresponding to an axon terminal. The intervening gap junction is labeled for Cx35 (10-nm gold beds). (A-D) Beneath these E-face images of gap junctions (green overlays), immunogold beads label Cx35 in the subjacent axon terminal plasma membranes. Yellow = putative glutamate receptor PSDs. A P-face

active zone of a glutamatergic synapse is opposite the PSD in A. Gold beads for Cx35 = 10-nm in A, B, and D, and 10-nm and 30-nm in C. SV = 50-nm synaptic vesicles in C. In attempt to improve immunogold labeling efficiency, we applied a 5-nm coat of carbon before the platinum layer; however, resolution in these images was also compromised. Calibration bars are 0.1 μm.

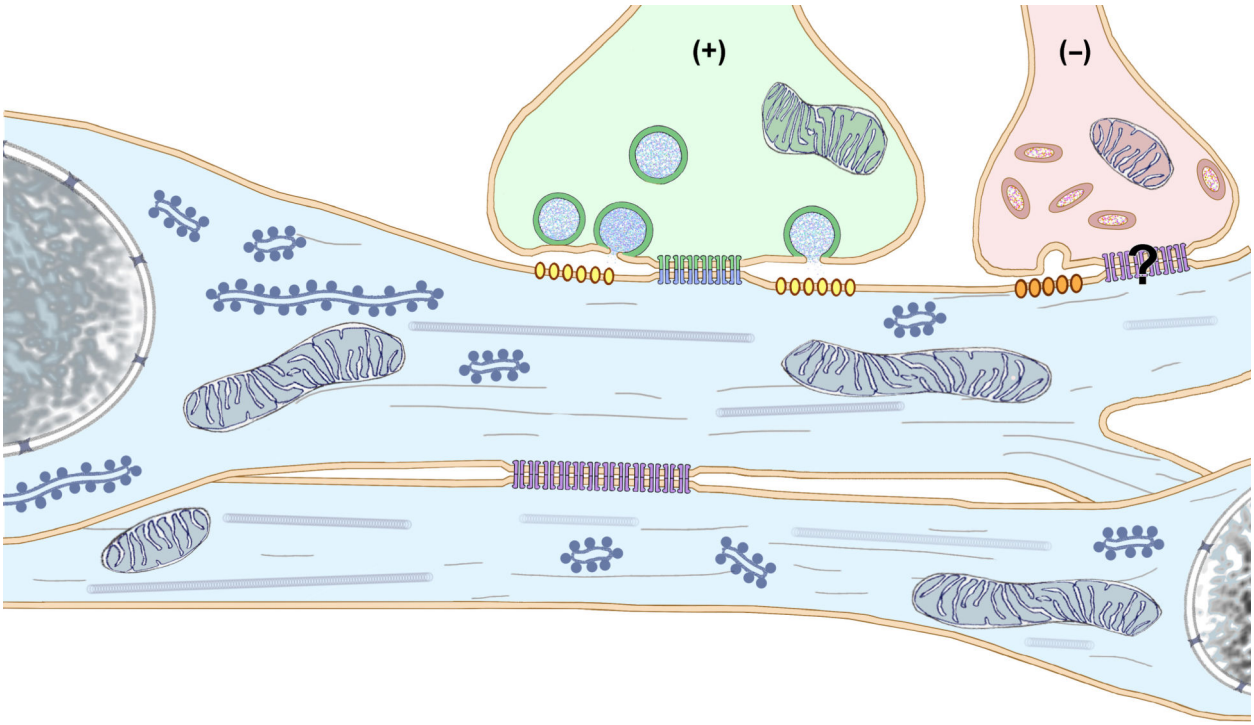

Fig. 14.

Diagram of different types of neuronal gap junctions and their connexins, as identified by FRIL in goldfish brain. Top center = glutamatergic mixed synapse (pale green overlay) onto neuronal dendrite (pale blue overlay), with presynaptic connexins (dark blue) in all glutamatergic mixed synapses identified as Cx35 by matched double-replica FRIL, and postsynaptic connexins (dark green) identified as Cx34.7. **(+)** = excitatory mixed synapse, identified by the presences of 50-nm round synaptic vesicles; **(−)** = inhibitory synapse, identified by presence of smaller (20-nm to 40-nm) flattened or “pleomorphic” synaptic vesicles (Nakajima et al., 1987; Peters et al., 1991; Legendre, 2001; Peters, 2014). (**?**) indicates that the existence of gap junctions linking inhibitory synapses of axon terminals to dendrites or axon initial segments is not yet determined, nor are their connexins identified, if such gap junctions exist. The connexins of purely electrical dendro-dendritic synapses (center; purple connexons) and of as yet hypothetical inhibitory mixed synapses (pink overlay; purple connexons), are not yet identified, but data in this report demonstrate that these latter two types do not contain Cx35 and suggest that few if any contain Cx34.7. With strong evidence for dendro-dendritic gap junctions in fish (Pappas and Bennett, 1966; Bennett et al., 1967a; Bennett et al., 1967b; Bennett et al., 1967c; Korn et al., 1977; Sotelo and Korn, 1978; Castelló et al., 1998), those gap junctions may be composed of connexins other than Cx35/Cx34.7, potentially including orthologs of mammalian Cx45.

Table

Relative level of antibody labeling by each of nine connexin antibodies in fluorescent puncta *vs.* in gap junction hemiplaques (immunofluorescence / FRIL).

Antibody *vs.* Connexin	**Ab298**	**Ab39-4200**	**Cx34.7 CT JOB 1263-2**	**Cx34.7 IL / JOB 2930***	**MAB 3043**	**MAB 3045**	**Ab37-4600**	**Ab51-6300**
Cx34.7	++ / ++	++ / ++	− to + / − to +**	− to + / − to +	− / −	− / −	− / −	− / −
Cx35	++ / ++	++ / ++	− / −	− / −	++ / ++	++ / ++	++ / ++	++ / ++
Species	Rabbit	Mouse	Chicken	Rabbit	Mouse	Mouse	mouse	rabbit

Relative connexin detection by each antibody is indicated by +'s or −. CT = carboxy terminus; IL = intercellular loop.

* = two different bleeds; purified bleed #1 has greater immunofluorescence labeling.

** strong FRIL labeling of postsynaptic connexons in zebrafish M-cell but weak labeling in goldfish M-cells;